MODAL AND HARMONIC ANALYSIS OF FREQUENCY CONVERTERS: A SIMULATION AND VALIDATION STUDY

Lappeenranta–Lahti University of Technology LUT

Master's Programme in Mechanical Engineering, Master's thesis

2024

Eetu Sukanen

Examiners: Professor Jussi Sopanen

Tuhin Choudhury, D.Sc. (Tech.)

ABSTRACT

Lappeenranta–Lahti University of Technology LUT

LUT School of Energy Systems

Mechanical Engineering

Eetu Sukanen

Modal and harmonic analysis of frequency converters: a simulation and validation study

Master's thesis

2024

75 pages, 35 figures and 12 tables

Examiners: Professor Jussi Sopanen and Tuhin Choudhury, D.Sc. (Tech.)

Keywords: Modal analysis, Harmonic analysis, Variable frequency drive, Vibration simulation, Environmental vibration

Industrial applications of machines have requirements to withstand environmental vibrations. These vibrations can affect the reliability and lifespan of products. These vibrations should be minimized in the design and validation phases of product development. In this thesis, the requirements and limitations of simulating environmental vibrations of a variable frequency drive (VFD) were considered. Emphasis was placed on the creation of a simulation model where base excitation is applied according to IEC standard environmental testing. These results were compared to existing experimental results of the same product. The model creation process was presented in detail and used theoretical background was covered. Additionally, environmental vibration simulation methods and implementations found in the literature were presented.

The results of the simulated modal and harmonic response analyses were used as the basis for conducting a sensitivity analysis for further understanding of the main parameters' impact on the simulation. The simulation results highlighted the accuracy and reliability of the results. It was found that simulation could be used to achieve a noticeable correlation with the actual VFD, although there were many factors causing uncertainty in the results and limiting accuracy. Many of these factors were analyzed and their significance was discussed.

Future research on the subject was discussed and potential gaps were identified for improving and gaining a better understanding of the subject. Overall, the thesis presented an overview of the accuracy and requirements for conducting environmental vibration simulation on a VFD. Additionally, the benefits and limitations of the methods and results were discussed.

TIIVISTELMÄ

Lappeenrannan–Lahden teknillinen yliopisto LUT

LUTin energiajärjestelmien tiedekunta

Konetekniikka

Eetu Sukanen

Taajuusmuuttajan modaalinen ja harmoninen analyysi: simulointi- ja validointitutkimus

Konetekniikan diplomityö

2024

75 sivua, 35 kuvaa ja 12 taulukkoa

Tarkastajat: Professori Jussi Sopanen ja Tuhin Choudhury, TkT

Avainsanat: Modaalianalyysi, Harmoninen analyysi, Taajuusmuuttaja, Tärinäsimulaatio, Ympäristön tärinä

Teollisuudessa käytettävillä laitteilla on vaatimuksia kestää ympäristön aiheuttamaa tärinää. Tärinä voi vaikuttaa tuotteiden luotettavuuteen ja käyttöikään. Tärinöiden minimointi tulisi toteuttaa tuotekehityksen suunnittelu- ja validointivaiheissa. Tässä työssä tutkittiin vaatimuksia ja rajoituksia ympäristön aiheuttaman tärinän simuloinnille taajuusmuuttajan näkökulmasta. Työssä painotettiin erityisesti simulointimallin luontia, jossa käytettiin perusherätettä ympäristön IEC tärinätestaus standardin mukaisesti. Työn tuloksia verrattiin vastaavaan olemassa olevaan kokeellisen testauksen tuloksiin. Mallin luomisprosessi esitettiin yksityiskohtaisesti ja käytetty teoreettinen tausta esitettiin. Tämän lisäksi esitettiin ympäristön tärinän simuloinnin metodeja ja toteutuksia kirjallisuudesta.

Modaali ja harmonisen analyysin tuloksia käytettiin pohjana herkkyysanalyysin toteutukselle, jotta voitiin saada syvempi ymmärrys käytettyjen pääparametrien vaikutuksesta simulaatioon. Tulokset korostivat simulaation tarkkuutta ja luotettavuutta. Työssä todettiin, että simulaatiota voidaan käyttää saavuttamaan tuloksia, joilla on merkittävä korrelaatio todelliseen laitteeseen, vaikkakin useat tekijät vaikuttivat tulosten varmuuteen ja rajoittivat niiden tarkkuutta. Näitä tekijöitä analysoitiin ja niiden merkityksellisyyttä pohdittiin.

Mahdollisia jatkotutkimuksia pohdittiin ja mahdollisia aukkoja tunnistettiin aiheen parantamiseksi ja syvällisemmäksi ymmärtämiseksi. Yhteenvetona työ esitti yleisen kuvan ympäristön tärinän simuloinnin tarkkuudesta ja vaatimuksista taajuusmuuttajille. Lisäksi työn hyötyjä ja rajoitteita pohdittiin.

ACKNOWLEDGEMENTS

I want to express big gratitude to ABB for facilitating the creation of the thesis. A special thanks to my thesis advisor, Janek Viman, for providing me with this amazing opportunity and for all the guidance throughout the research. I would like to thank my supervisors Jussi Sopanen and Tuhin Choudhury for all the excellent and invaluable guidance and support on the thesis.

Lastly, I am very grateful for all the help and support my family and friends have provided me throughout my studies. Special thanks to those with whom I have had the pleasure of sharing the best moments of this journey and from whom I have gained the best memories that I will hold dear for the rest of my life.

Eetu Sukanen

Espoo 30.11.2024

SYMBOLS AND ABBREVIATIONS

Roman characters

C	Damping matrix	kg/s
F_0	Force amplitude	N
K	Stiffness matrix	N/m
M	Mass matrix	kg
t	Time	s
x	Deformation	m
$\dot{x}$	Speed	m/s
$\ddot{x}$	Acceleration	m/s^2

Greek characters

α	Rayleigh alpha coefficient	1/s
β	Rayleigh beta coefficient	s
Ω	Natural frequency	rad/s
ω	Natural frequency	rad/s

Constants

g	gravitational acceleration	10 m/s^2

Dimensionless quantities

i	Mode index
r	Mode index

ζ	Damping ratio
Ψ	Eigenvector

Abbreviations

CAD	Computer-Aided Design
DoF	Degree of Freedom
EoM	Equation of Motion
FE	Finite Element
FEA	Finite Element Analysis
FEM	Finite Element Method
Hz	Hertz
IEC	International Electrotechnical Commission
MDoF	Multi Degree of Freedom
MP	Measurement Point
PCB	Printed Circuit Board
SDoF	Single Degree of Freedom
VFD	Variable Frequency Drive

Table of contents

Abstract

Tiivistelmä

Acknowledgements

Symbols and abbreviations

1 Introduction 9
1.1 Research problem 10
1.2 Research questions 11
1.3 Objective 12
1.4 Scope 12
1.5 Thesis structure 12
2 Theoretical background and literature review 14
2.1 Theoretical basics of forced vibration 14
2.2 Literature review: Simulation of vibration testing 18
2.2.1 Virtual test simulation 19
2.2.2 Virtual test simulation implementations 22
2.2.3 Experimental vibration analysis 27
3 Case study: Vibration simulation of a variable frequency drive 28
3.1 Experimental setup 28
3.2 Used software 29
3.3 Model creation 30
3.4 Modal analysis 39
3.5 Harmonic response 40
3.6 Sensitivity analysis 43
3.7 Result post-processing 45
3.8 Simulation validation and reliability 46
4 Results 47
4.1 Modal analysis 47

4.2 Harmonic response 48
4.3 Frequency and acceleration error 50
4.4 Results of the sensitivity analysis 52
5 Analysis and discussion 60
5.1 Analysis of the initial simulation results 60
5.2 Analysis of the results of the sensitivity analysis 60
5.3 Analysis of the final results 61
5.4 Validity and reliability of the results 66
5.5 Limitations 69
6 Conclusions 71
References 73

1 Introduction

Effectively all electronic equipment experiences vibration. The sources, frequencies, and accelerations of vibrations vary widely. The experienced vibrations can change depending on the stage of the product's life cycle, such as transportation, installation, and active use. (Steinberg 2000, p. 1.)

Variable frequency drives (VFD) are power electronics used for controlling electronics, especially electric motors. Their ability to dynamically adjust the speed of electric motors offers higher control over the behavior of the machine and the added benefit of reduced energy consumption and environmental impact. Variable frequency drives are applied in different industries and the use cases of VFDs include pumps, electric vehicles, propulsion systems, milling, etc. (Bose 1997, p. 1-2.) Figure 1 shows an ABB variable frequency drive.

Figure 1. ABB variable speed drive ACS580-01-09A5-4+B056 (Sahkonumerot 2024).

Different industrial applications for frequency converters (variable frequency drive) have environmental requirements to withstand external vibrations. Environmental vibrations can come from a multitude of sources, such as the eccentricity of large motors, vehicle ground contact, wind-induced stresses, and earthquakes. Large motors often cause sinusoidal vibration to their operating environment which can excite other machines near it. (Steinberg 2000, p. 10-16.)

The vibration resistance of the products should be considered in the design of the product in environments where induced vibrations are significant. In these cases, frequency converters must adhere to requirements and standards that determine the maximum allowable displacement amplitudes during vibration testing. If a machine experiences large enough excitation at resonant frequencies, the operation can be disrupted, fatal structural damage can occur via large deformations and loads, or fatigue of critical components can happen. Failure to meet such requirements requires redesign or augmentation of the product to achieve compliant results. (Kurowski 2016, p. 219.)

Finite element analysis (FEA) is a numerical method that can be used to simulate the physical behaviors of products and components. Using computer software allows for calculating very complex models, which would be impossible by hand. The ability to utilize FEA in product design makes it very useful for analyzing properties such as vibration before physical prototyping. (Kurowski 2016, p. 1.)

1.1 Research problem

Product development process creates a large library of 3D modelled components for the purpose of manufacturing and assembly. Utilizing these CAD models for vibration simulation presents a challenge and requires additional effort and adaptation. Often the CAD models are compatible to be utilized in FEA, but this is not a guarantee and even a few components out of a larger assembly can cause problems. A separate simulation model needs to be developed based on the 3D models. (Kurowski 2016, p. 209.)

The main research problem is the lack of knowledge about the feasibility and efficiency of implementing a vibration simulation on entire product assemblies in the context of product development and whether results from finite element analysis correspond to experimental

results. Most studies on the subject mainly focus on component-level analysis. Louback, Mistry, Azer & Bilgin (2022, p. 7-12) created a study on simulating modal and harmonic analyses on a traction inverter and its housing. They similarly noted that only a few papers have discussed vibration analysis of traction inverters which have similar structural properties as VFDs.

It is not fully understood how well these 3D models can be adapted or what the actual required workload is for a successful implementation. Furthermore, the inclusion of small components and connectors increases the computational load and required design effort for model creation, which encourages finding a good balance for the accuracy of the model. Adapting these models for vibration analysis, especially modal and harmonic analysis, presents challenges as they are often not directly applicable to be used in simulation.

According to Palmieri, Cianetti, Zucca, Morettini & Braccesi (2021, p. 1), sine sweep testing is typically used in specific industries, such as automotive and aviation. Research on virtual simulation of the sine sweep vibration testing is limited. (Palmieri et al. 2021, p. 1.) Limited research and use of sine sweep environmental vibration simulation in other industries reinforces the importance of researching the topic, especially researching in the context of variable frequency drives.

1.2 Research questions

The thesis aims to provide a solution to the research problem by answering relevant research questions. The research questions are formulated to cover aspects of the thesis topic. The research questions of the thesis are as follows:

- How accurately can a simulation predict the behavior of a variable frequency drive experiencing environmental vibration, and how well it compares to experimental results?
- How sensitive are the results of the simulation to changes in the simulation's key parameters such as mesh size and boundary conditions?
- What are the limitations vibration simulation presents for frequency converter designing and testing?

1.3 Objective

The main objective of the thesis is to analyze and understand the methods of simulating environmental vibrations as a means of complying with the IEC 60068-2-6 environmental testing standard. The study focuses on the utilization of vibration simulations for modal and harmonic analysis to evaluate the expected behavior of variable frequency drives under practical operation conditions.

For further information on the objective, a case study of a variable frequency drive will be conducted. The methodology and results of the case study are used to evaluate the feasibility and accuracy of the simulation. Experimental environmental testing results of the same product are used as the basis for validating the simulation and setting the simulation parameters.

In conclusion, the thesis aims to explore whether environmental vibration simulation is comparable to experimental testing, and how the used methods can be applied and utilized in the product development of frequency converters.

1.4 Scope

The scope of the literature review is limited according to the top-down approach of virtual testing of environmental vibrations, according to which the vibration simulation and experimental testing are also then covered.

The scope of the case study is determined by the IEC 60068-2-6 environmental testing standard. The standard is used to determine the vibration simulation test environment and excitation. The standard consists of a frequency sweep of the product where the natural frequencies are determined.

1.5 Thesis structure

The thesis begins with an introduction to the topic by covering theoretical basics of forced vibration and a literature review on vibration simulation and especially environmental vibrations. In this thesis, a vibration analysis containing modal analysis and harmonic

analysis of a frequency converter is conducted and the process of simulating such analysis is discussed in terms of the whole design stage of product development. The case study of the VFD vibration testing is conducted according to the methods outlined by the theoretical background and the presented simulation methodology. The validity of the simulation results is evaluated by conducting a sensitivity analysis and comparing results to previously gathered experimental testing results. Additionally, a literature review of the topic of vibration analysis simulation is conducted. The literature review is used to establish a better understanding of the current state of environmental vibration analysis simulation and its main applications. In the final part of the thesis, the final conclusions of the study are presented. The main findings of the thesis and their importance are evaluated and possible future research topics on the subject are proposed.

2 Theoretical background and literature review

The methods chapter presents the theoretical basics of modal and harmonic analysis, especially on frequency domain response analysis. Additionally, a literature review on the thesis topic with brief information on the subject background is presented.

2.1 Theoretical basics of forced vibration

In this chapter the theoretical concepts used in the vibration simulation are presented. Overview of the used equations in modal analysis and harmonic analysis are covered. These concepts are critical in understanding the underlying theory behind the FEA conducted later in the case study.

The following equation presents the equation of motion (EoM) for a free multi-degree of freedom (MDoF) vibration system. The following equation represents the dynamic behavior of a basic free undamped system.

$$\mathbf{M}\ddot{\mathbf{x}} + \mathbf{K}\mathbf{x} = 0 \tag{1}$$

Matrix **K** represents the stiffness matrix of the system and matrix **M** is the mass matrix of the system. Acceleration $\ddot{\mathbf{x}}$ represents the acceleration of the system and **x** represents the displacement of the system. (He & Fu 2001, p. 55.)

The square roots of the eigenvalues and the eigenvectors represent the natural frequencies and mode shapes of the system, respectively. Eigenvalue problem is presented in the following equation:

$$\left(\mathbf{K} - \omega_i^2\mathbf{M}\right)\mathbf{\Psi}_i = 0 \tag{2}$$

Matrix **K** represents the stiffness matrix of the system. Matrix **M** is the mass matrix of the system. Omega $\boldsymbol{\omega}_i$ represents the eigenvalue and $\boldsymbol{\Psi}_i$ represents the eigenvector of the system, where i represents the index of a mode. (He & Fu 2001, p. 94.)

Most vibration analyses consider linear vibration analysis. Nonlinear vibration analysis is used in cases where the displacements are large, and material behaves with nonlinear properties. Modal superposition is a method used in linear vibration analysis to significantly decrease the complexity and computation load of the analysis. (Kurowsk 2016, p. 183, 190.)

Modal damping ratios cannot be determined by using finite element analysis and therefore experimental measurements need to be used. Measurements provide a modal damping ratio for multiple modes. Finite element analysis software often allows for input of a single modal damping ratio in which case the modal damping ratio is calculated from the average of measured damping ratios in various boundary condition installations. (Lee, Wang, Lai, Yeh & Chen 2008, p. 1845.)

Modeling of damping ratios is difficult and is one of the main challenges in the modeling of damped MDoF systems. Proportional damping is often used to simplify the system to allow successful analysis. Proportional damping consists of a damping ratio which is assigned for each mode of the system. The following equation presents the calculation of a damping matrix using Rayleigh damping coefficients (He & Fu 2001, p. 123):

$$\mathbf{C} = \alpha\mathbf{M} + \beta\mathbf{K} \tag{3}$$

The equation determines the damping matrix **C** using a proportional damping ratio. The damping matrix consists of the Rayleigh damping coefficients α and β, which are used as coefficients for the mass matrix **M** and the stiffness matrix **K**, respectively. The Rayleigh damping coefficients are calculated from the following equation (He & Fu 2001, p. 124):

$$\zeta_r = \frac{\alpha}{2\omega_r} + \frac{\beta\omega_r}{2} \tag{4}$$

The damping coefficients are constants which can be calculated from the damping ratio ζ of the system for a certain mode r and its natural frequency ω_r. The two coefficients are derived from equation (4). Introducing damping to the equation of motion of a MDoF system results in the following equation (He & Fu 2001, p. 124):

$$\mathbf{M}\ddot{\mathbf{x}} + \mathbf{C}\dot{\mathbf{x}} + \mathbf{K}\mathbf{x} = 0 \tag{5}$$

In cases where the damping ratio of the system is provided a proportionally damped MDoF system can be used. The EoM for the system consists of a damping matrix **C**, a stiffness matrix **K** and a mass matrix **M**. Additionally, the acceleration $\ddot{\mathbf{x}}$, speed $\dot{\mathbf{x}}$ and displacement **x** of the system are used as variables. (He & Fu 2001, p. 124.)

The use of the mode shape matrix allows for the mass matrix **M** and the stiffness matrix **K** to be diagonal. Diagonal matrices provide an important property of each mode shape being uncoupled. The damping matrix **C** is a coupled matrix which complicates the solving of the EoM. Using Rayleigh coefficients, the damping matrix can be uncoupled which is very important for being able to solve the EoM for each mode shape individually. (He & Fu 2001, p. 124.) The following two equations are derived from equation (4) by He & Fu (2001, p. 124) and outline the calculation of the Rayleigh coefficients in the case of global damping, where a single damping ratio is used to represent the damping behavior of the system. Overall, the calculations required for vibration analysis can be simplified significantly when utilizing a global damping ratio.

$$\zeta = \frac{\alpha}{2\omega_1} + \frac{\beta\omega_1}{2} \tag{6}$$

$$\zeta = \frac{\alpha}{2\omega_2} + \frac{\beta\omega_2}{2} \tag{7}$$

The Rayleigh coefficients need to be calculated for each mode separately when the respective damping ratios are known. Equations (6) and (7) present the calculations for Rayleigh coefficients in the case of a global damping ratio ζ for two mode shapes. Omega ω_r represents the respective natural frequencies of two modes. The following three equations outline the steps to acquiring individual equations for each coefficient:

$$\alpha = 2\zeta\omega_1 - \beta\omega_1^2 \tag{8}$$

$$\zeta = \frac{2\zeta\omega_1 - \beta\omega_1^2}{2\omega_2} + \frac{\beta\omega_2}{2} \tag{9}$$

$$\beta = \frac{2\zeta(\omega_2 - \omega_1)}{(\omega_2^2 - \omega_1^2)} \tag{10}$$

First using equation (6) the alpha coefficient α is solved, which is presented in equation (8). Then substituting the alpha coefficient in equation (7) with equation (8), the beta coefficient β can be calculated as shown in equation (10). Finally, the alpha coefficient can be calculated by solving for alpha with the value of the beta coefficient, shown in equation (8).

Excitation can generally be considered to be either harmonically forced excitation or base excitation. In base excitation, the excitation forces are not directly applied to the main subject, but rather to the base, foundation, or support of the object. The loading forces are passed through the base to the object to simulate environmental vibration such as earthquakes. (Benaroya, Han & Nagurka 2022, p. 119.) When modeling vibration analysis with base excitation, the boundary conditions between the base and the structure are critical in affecting the results of the analysis. The following equation presents the EoM for a MDoF harmonic response, where harmonic excitation of the system is present:

$$\mathbf{M}\ddot{\mathbf{x}} + \mathbf{C}\dot{\mathbf{x}} + \mathbf{K}\mathbf{x} = F_0 e^{i\Omega t} \tag{11}$$

It consists of a damping matrix **C**, a stiffness matrix **K** and a mass matrix **M**, and used variables are the acceleration $\ddot{\mathbf{x}}$, speed $\dot{\mathbf{x}}$, displacement **x**, force amplitude F_0, specific frequency Ω, index i and time t. The equation of motion is used for harmonic excitations, for example the sinusoidal vibration, where steady state behavior is assumed. (Cai 2016, p. 403.) Harmonic response analysis is used to calculate the response of a system experiencing sinusoidal loading. This can be used to determine systems behavior at a certain frequency range, for example, the amplitudes of displacements especially at the natural frequencies. (Ansys 2023, p. 469.)

Mode superposition is often used in harmonic response analysis to simplify the calculations. In mode superposition, the results of a modal analysis are used as initial loading conditions for the system. This method allows for multiple harmonic analyses to share the same initial modal analysis, therefore reducing the computation time. (Ansys 2023, p. 469.)

Frequency response plotting of displacement amplitudes requires the calculation of total deformation amplitudes. Calculating the amplitude of total deformation is presented in the following equation (Ansys 2023, p. 478):

$$|u_{total}| = \sqrt{(u_{total})^2_{real} + (u_{total})^2_{imag}} \tag{12}$$

The equation combines the total deformation of both the real and imaginary components of the total displacement (Ansys 2023, p. 478).

2.2 Literature review: Simulation of vibration testing

In this chapter, a literature review of the thesis topic is conducted utilizing research from LUT-Primo, Scopus, and Google Scholar databases. Basic theory on vibration and the experimental analysis process methods are covered. Various industry and academic implementations and their conclusions of vibration simulation are presented.

Computer simulation of vibration is generally done with the finite element method. FEM is a method that approaches the numerical solution of a wide array of physical phenomena,

such as vibrations, from an individual element level. Individual elements are interconnected to each other with boundary conditions and constraints. Connecting and combining each individual element into a single model creates large matrices for calculating system behaviors. When using assembly algorithms the large matrices, such as mass matrices and damping matrices, are used to calculate the behaviors and properties of each individual node of the model. (Palazzolo 2016, p. 637.)

2.2.1 Virtual test simulation

Virtual testing is used to simulate the testing process of components and products. The process of virtual testing focuses on creating accurate testing environments equivalent to physical testing. (Gorskii, Gavrilov & Borovkov 2020, p. 1.) Virtual testing using finite element methods (FEM) is used as an alternative or in conjunction with experimental testing (Guerrero, Sasikumar, Llobet & Costa 2023, p. 1). One of the main uses of virtual testing is to provide understanding and insight into the expected behavior during actual testing. Knowledge gained from virtual testing is then used to improve the design of the product before physical testing, providing valuable time and cost savings. (Gorskii et al. 2020, p. 1.; Bruetsch & Delima 2023, p. 87.)

Virtual testing provides additional accuracy to simulation results when compared to just traditional simulation analysis. This increased accuracy can be critical in the pursuit of realistic results. (Gorskii et al. 2020, p. 1.)

The process Cianetti, Morettini, Palmieri & Zucca (2019, p. 528) used for developing a component while utilizing vibration simulation is detailed in Figure 2. The process consists of 4 parts, materials, finite element modeling, lab structural dynamics, and field structural dynamics. The link between FEM and experimental analysis describes how the dynamic model and validation of the prototype is used as an iterative process to achieve validation of the qualification test.

Lee et al. (2008, p. 1838) presented a process flowchart for verification of vibration simulation finite element analysis. The procedure is aimed at creating an equivalent finite element model to the experimental testing results. The process flowchart is presented in

Figure 3. The flow chart shows the traditional way of validation where the experimental testing is done simultaneously with the simulation.

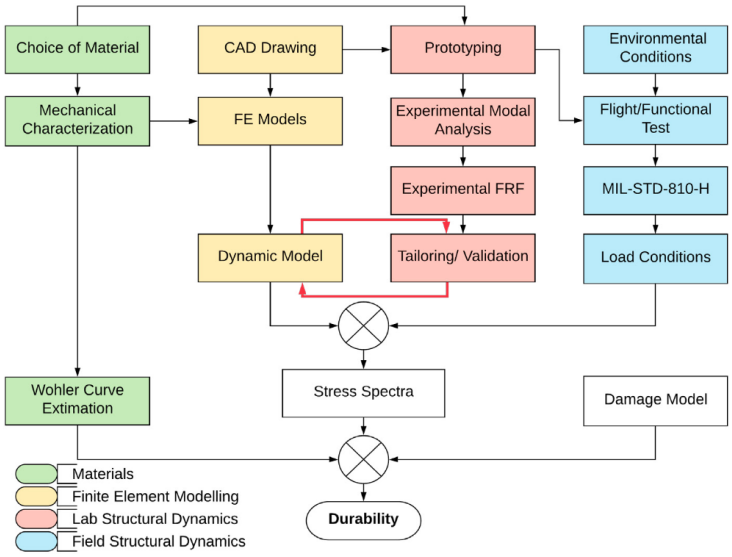

Figure 2. Process flowchart for the methods used for materials, finite element modeling, lab structural dynamics, and field structural dynamics (Cianetti et al. 2019, p. 528).

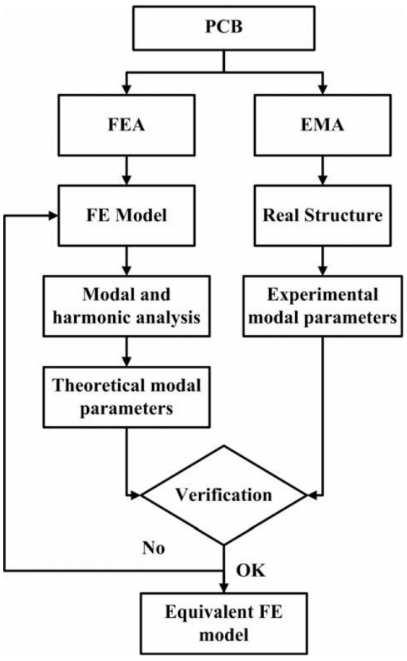

Figure 3. Flowchart of a vibration simulation FEA verification process with experimental data for a PCB (Lee et al. 2008, p. 1838).

The virtual simulation process used by Remedia, Aglietti, Appolloni, Cozzani & Kiley (2017, p. 182) is presented in Figure 4. The diagram details the flowchart used to arrive at an adequate correlation between the virtual testing of the finite element model and the testing data. The dotted lines represent the added virtual testing workflow designed to improve the accuracy of the testing.

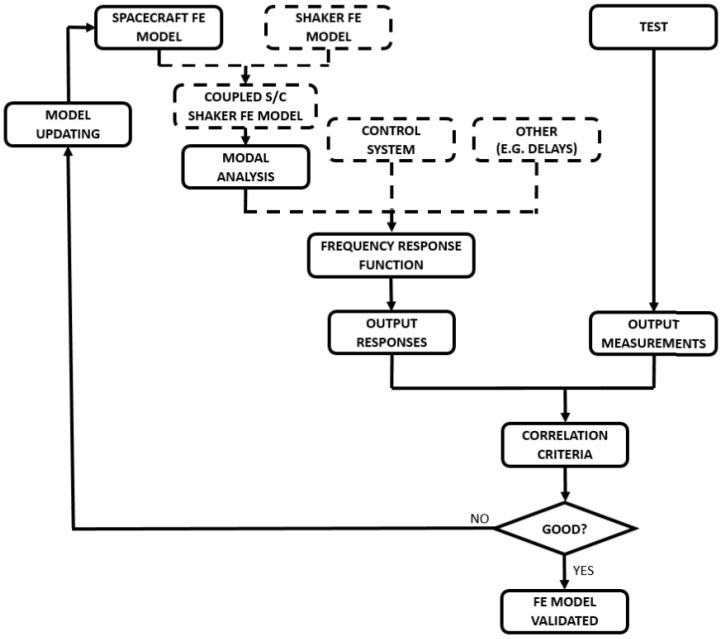

Figure 4. Diagram for a finite element vibration validation process. The dotted lines represent the improved workflow which includes virtual testing. (Remedia et al. 2017, p. 182.)

Dong & Shang (2019, p. 170) presented the process flow and corresponding actions between the experimental and virtual testing in Figure 5. The diagram details the equivalent actions in experimental testing in comparison to simulation.

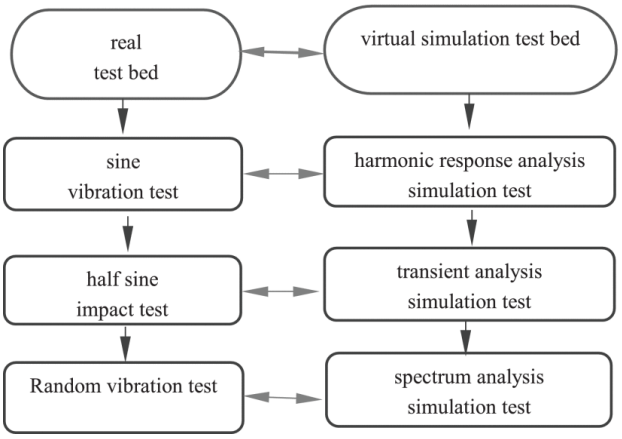

Figure 5. Process flow and relations between the experimental and virtual testing (Dong & Shang 2019, p. 170).

Essentially all the processes used by the presented studies use the experimental results to validate the simulation results. By iteration of the simulation, the accuracy of the results is achieved. The exclusive use of only simulation is rarely used as validation due to the high sensitivity and uncertainty of vibration simulation.

2.2.2 Virtual test simulation implementations

This chapter presents implementations of virtual testing simulation found in the literature. The emphasis of these research papers was on the significance of creating vibration testing simulations that try to mimic the behavior expected from the actual experimental vibration tests.

Cianetti et al. (2019) demonstrated that the simulated test qualification process in the aerospace industry is a viable option to decrease the likelihood of failure in actual testing. A frame consisting of two components bolted together was simplified and modeled. Using the finite element method a mesh of the 3D model was created, then modal analysis was conducted, and natural frequencies of the frame were acquired. Figure 6 shows the achieved correlation between the numerical and experimental results. The Figure shows a clear correlation, especially in the lower natural frequencies. The least accurate parts of the results are in the higher frequency range.

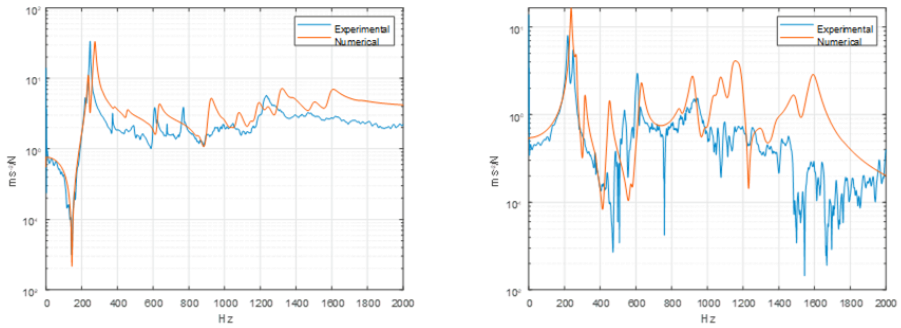

Figure 6. Frequency response plot where both numerical and experimental results are shown (Cianetti et al. 2019, p. 531).

Remedia et al. (2017) tested and evaluated the feasibility of virtual testing as a tool for spacecraft design. The correlation between real test results and simulation was proven to be significant. The simulation results were significantly improved by modeling and simulating the shaker and coupling it with the measured object. Notably, when compared to similar finite element models the virtual testing results were proven to be more accurate. The insides of the actual shaker and corresponding CAD model are presented in Figure 7.

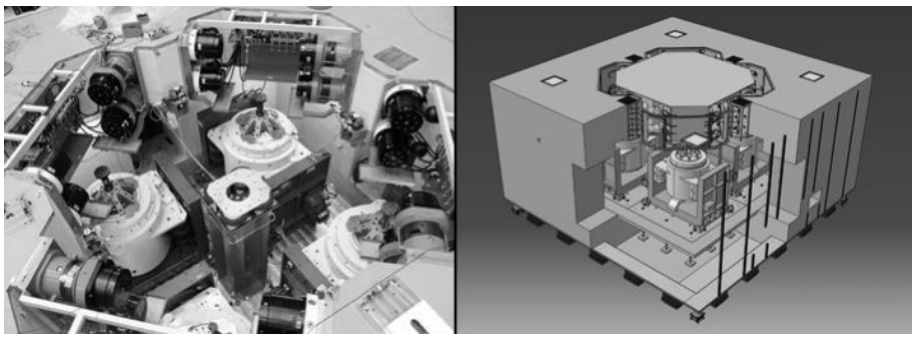

Figure 7. Electro-dynamic vibration shaker, where left side represents the actual shaker and right side represents the CAD model (Remedia et al. 2017, p. 188).

A similar study on virtual testing by Remedia, Aglietti & Kiley (2015, p. 9) conducted a simulation of an electro-dynamic vibration shaker, where the final results are compared between the experimental testing, FEA and virtual testing. Utilizing virtual testing methods

improved the accuracy of the frequency response of the system. Figure 8 presents a comparison plot of the shaker where all three different methods are plotted.

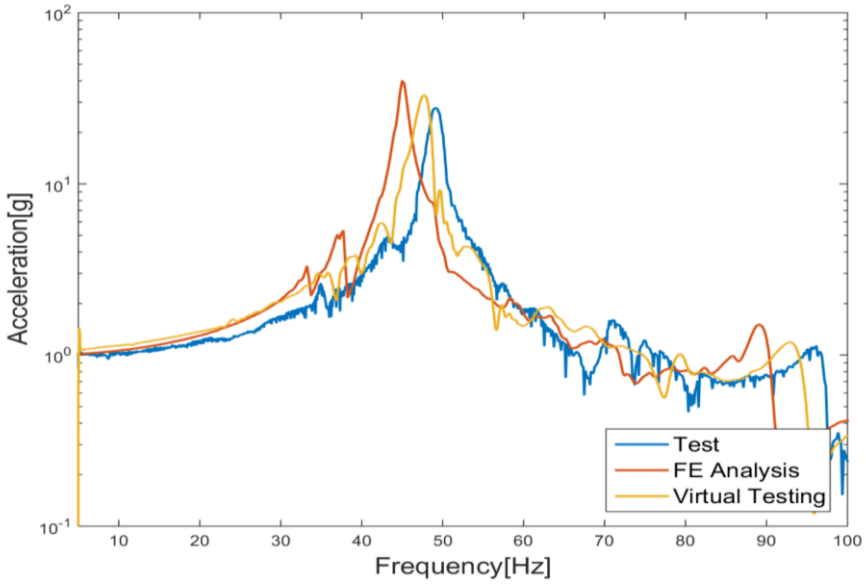

Figure 8. Frequency response plot of experimental, FEA and virtual testing of a shaker table (Remedia et al. 2015, p. 9).

Martino & Harri (2019) developed a model of an electrodynamical exciter using a mathematical model and concluded its suitability for virtual testing. The simulation results were validated with experimental results and a good correlation between them was noted. They noted that experimental tests are still essential in product development, but virtual simulation methods could be used as tools to optimize and provide initial design validation before actual testing. In Figure 9 the shaker components and a vibration model diagram are presented.

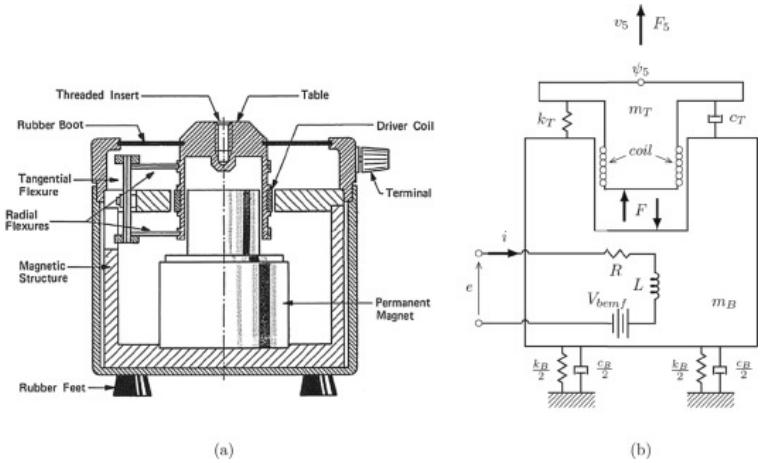

Figure 9. Description of a modeled vibration shaker. The left side presents the shaker components, and the right side the vibration model diagram. (Martino & Harri 2019, p. 7.)

Guerrero et al. (2023) conducted experimental and virtual testing of an aircraft wing box. In the study, the assembly was manufactured and tested using traditional experimental testing methods. Additionally, a finite element model was created to simulate the thermal behavior of the assembly. The results of the simulation agreed with the experimental results, especially in deformation shapes. The two results did have absolute differences, and some parts of the simulated assembly had a better correlation to actual results than others. Overall, it was concluded that the finite element approach to testing is a viable option and that the results had a reasonable correlation. Figure 10 shows the CAD model and actual wing box representations and the accompanying shakers.

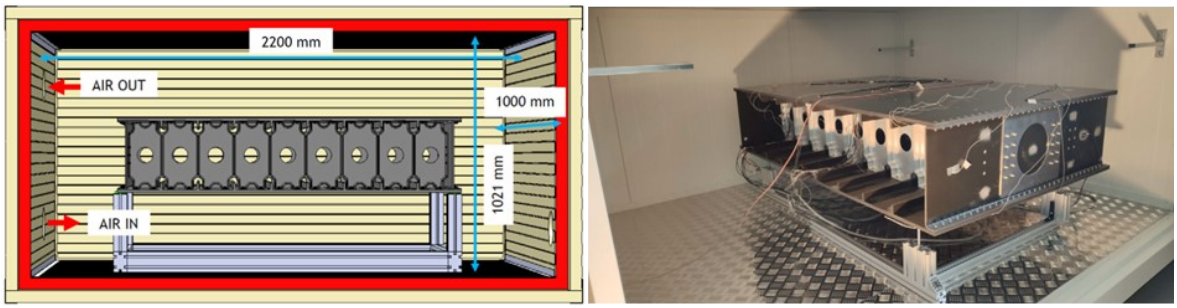

Figure 10. Representation of the shaker and component, where left side represents the CAD model, and right side represents the actual wing box (Guerrero et al. 2023, p. 4).

Dong & Shang (2019, p. 169-173) conducted a virtual simulation of high-speed electric multiple-unit electronic equipment. The virtual simulation was used to test the natural frequency, sinusoidal vibration, semi-sinusoidal impulse, and random vibration. It was noted that virtual test simulation had a shorter test cycle when compared to experimental testing and had better applicability in the simulation of extreme environments.

Bruetsch & Delima (2023, p. 87-89) created a simulation of an electromagnetic shaker. The simulated shaker was considered as a replacement for experimental testing. The study noted that the behavior of an actual shaker was successfully recreated with reasonable accuracy. The study noted that this was achieved after successfully finding out how damping and boundary conditions should be applied, which the study noted as the main challenges. The modal damping was applied to each eigenmode individually, with the first mode receiving the highest damping and progressively decreasing for the following modes. Additionally, having accurate boundary conditions was found critical in achieving good results. If the model was too stiff the natural frequencies would be incorrect. The achieved result comparison with experimental results is demonstrated in Figure 11.

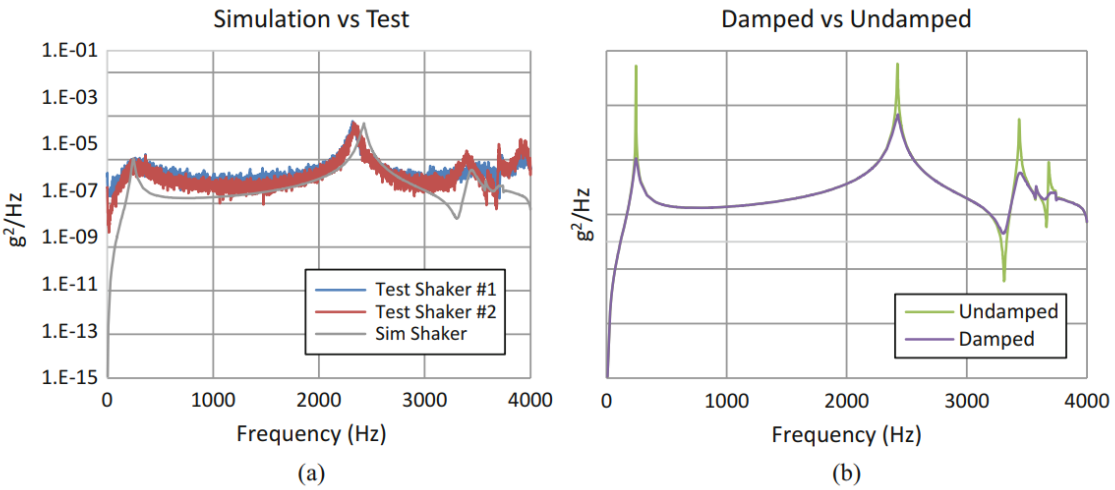

Figure 11. The left side represents a frequency response plot where simulation results are compared to experimental results. On the right a comparison between undamped and damped simulation results is presented. (Bruetsch & Delima 2023, p. 89.)

2.2.3 Experimental vibration analysis

Vibration analysis testing often requires a machine that excites the test subject. One of the most common methods is an electrodynamic shaker. The shakers allow for excitation that simulates harmonic motion. (Steinberg 2000, p. 346.)

Determining the damping of a system using finite element analysis is very difficult. Often the damping is first measured using experimental analysis after which it can be used in the simulation. (Brandt 2010, p. 4.)

The international standard IEC 60068-2-6 (2007, p. 7) outlines methods for conducting sinusoidal vibration testing. Requirements for the harmonic load testing are specified. The testing methods include guidelines for the motion and tolerances for conducting testing. The test consists of two main phases, frequency sweep and endurance testing.

The sweeping phase of the test includes going through frequencies within the limits of the testing frequency range. The frequency is set to change exponentially with respect to time, where the factor of exponential growth is determined as octaves per minute. (IEC 60068-2-6 2007, p. 12.)

Endurance testing at critical frequencies is conducted for each axis. Duration for the endurance testing varies from 10 minutes to 10 hours. Measuring the vibration testing should be done by measuring the object from its fixing points, to be used as reference points, and other points of interest where the largest loads are expected, or critical components are located. (IEC 60068-2-6 2007, p. 8, 18.)

3 Case study: Vibration simulation of a variable frequency drive

In this chapter the experimental setup used for acquiring the reference experimental results is first presented. The used equipment and testing methods are covered. The methods for creating a vibration simulation of a variable frequency drive are then presented. Each of the modeling steps, model creation, modal and harmonic analysis, sensitivity analysis and result post-processing is presented. The modeling process is covered in the order of execution. Additionally, the principles by which the validation and reliability of the simulation is measured are presented. The basic principles and equations of motion and multi-degree of freedom vibration are presented in chapter 2.1 of the thesis.

3.1 Experimental setup

The experimental testing on the case study VFD was previously conducted by an external laboratory commissioned for standard compliance testing. The testing included two other drives that were simultaneously tested using a large aluminum jig. The testing set up is presented in Figure 12. The figure shows all three VFDs and the jig.

The testing was conducted using an electrodynamic shaker LDS V875. The shaker provided the sinusoidal base excitation to the system with controlled acceleration in the given frequency range. In addition, B&K 4371 accelerometer was used to measure the amplitudes in the testing.

The experiment was controlled using software which allowed for IEC 60068-2-6 standard compliant acceleration profile to be applied to the system. The testing parameters were set according to the IEC standard. The test went through a frequency range of 10 Hz to 150 Hz, where the base excitation amplitude rose to 1 g between 10 Hz and 57.56 Hz. The sweep rate of the test was 1 octave per minute. The experimental measurement results are presented with an uncertainty of ±5%.

Figure 12. The experimental setup used in environmental testing, which includes other tested products.

3.2 Used software

The case study requires a suite of software to execute the vibration analysis of a variable frequency drive. This software includes CAD software, FEM software, FEM solvers, and post-processing data analysis software. Each of the used programs is presented.

The first 3D CAD software used is Creo 7. The original model data for the geometry used in the case study is made and saved in Creo format ".prt" or ".asm". The second 3D CAD software used in the case study is Ansys SpaceClaim. SpaceClaim is a CAD system that is specifically designed to be simple to learn and efficient at preparing geometry to be used in Ansys simulation modeling (Ansys 2024a).

Ansys Mechanical is a finite element analysis software that is used to model and solve the modal and harmonic analysis of the case study (Ansys 2024b). Ansys Parametric Design

Language (APDL) is used to communicate with the Ansys mechanical solver. The solver is used to run the finite element analysis and is the underlying engine. (Ansys 2024c.)

ANSYS Workbench is a platform used to integrate Ansys engineering solutions such as Ansys SpaceClaim and Ansys Mechanical (Ansys 2024d). Ansys Workbench is used to create and organize the case study as a single project.

3.3 Model creation

The creation of the vibration analysis model begins with acquiring sufficient geometry data. In the case of the variable frequency drive, a 3D model assembly consisting of all assembled parts is used. The model is first exported in ".stp" file format and imported into Ansys SpaceClaim CAD software. The imported geometry can be seen in Figure 13.

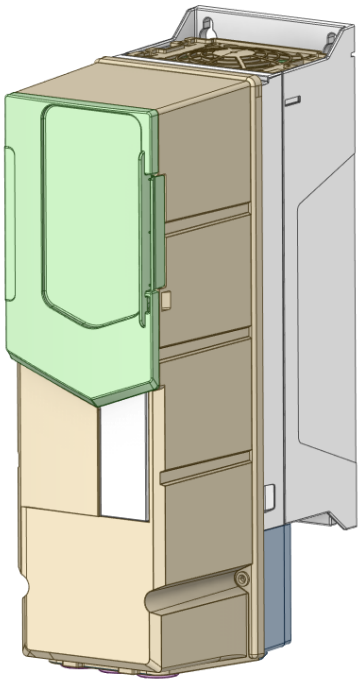

Figure 13. Imported VFD geometry in SpaceClaim.

An important step in importing the geometry data is choosing which components should be included. The aim of the model is to provide the structural frame for the finite element model.

Only mechanically and structurally important components should be included, in addition to components that provide meaningful weight to the system. (Kurowski 2016, p. 89.)

The imported geometry includes many unnecessary and minor components, such as stickers and text plates which can be suppressed or deleted from the geometry. Including these in the model would require modeling the connections and material properties. They would also further complicate the mesh structure and increase the mesh size significantly due to the high level of detail associated with them.

The assembly includes a large number of fasteners that are not used in the modeling. The inclusion of the fasteners in the geometry is beneficial since they can be used to indicate where connections between components should be modeled. Each fastener needs to have two arcs or edges as reference which are used to create the beam connection. These edge features should be grouped as selections in SpaceClaim to be used later in automated finite element model connector creation. This is not strictly necessary but helps to reduce the manual workload in creating possibly hundreds of connections.

For further assistance in modeling the components can be grouped into many sub-assemblies to aid in the organization and connection creation in the future. Some examples of the grouping include outer casing, inner casing, heat exchanger, and circuit boards 1 and 2. If the entire VFD assembly includes hundreds of components it can be difficult to create entire model simultaneously. Creating the model by completing the sub-assemblies separately helps in handling the large number of connections and components.

Some errors and imperfections may transfer over or arise to the geometry in the export process which can require fixing. An imported geometry often needs to be fixed, and bad quality geometry features need to be removed. These include small faces that have appeared in the importing phase of the CAD geometry. These small features can be for example, chamfers, small angles or sharp edges. (Kurowski 2016, p. 213.) SpaceClaim includes a multitude of tools and options for approaching fixing these errors and imperfections in the geometry.

Further optimizations to the geometry can be done with the model preparation tools provided by the Ansys SpaceClaim software. Some components include embossed text and features that are not structurally significant but increase the level of detail required for accurate meshing. These features can be removed by simply highlighting and deleting them. This

process is manual and can be time consuming, but the resulting mesh simplification provides a good incentive. A before and after feature removal is presented in Figure 14.

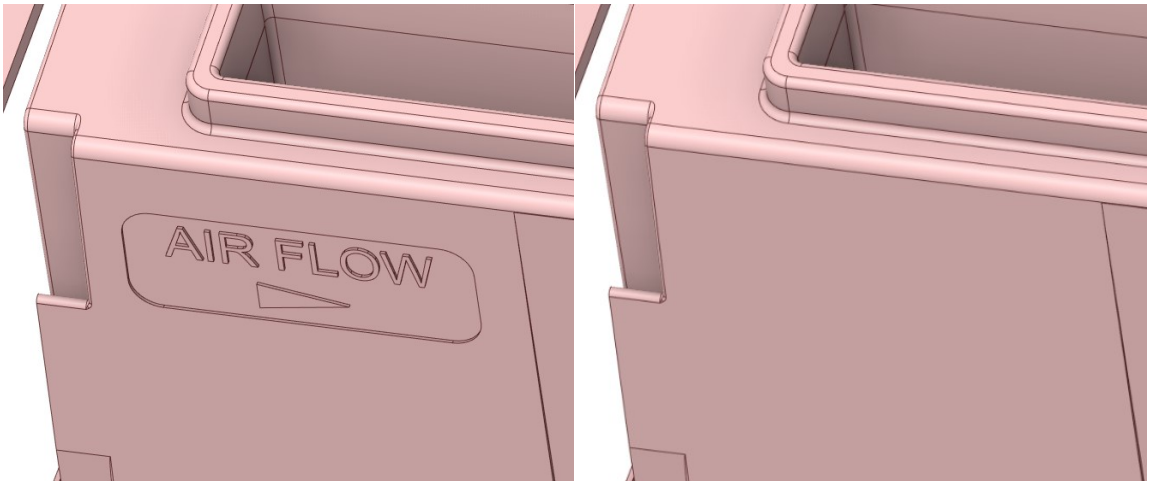

Figure 14. An example of a before and after of the geometry feature removal in SpaceClaim. The embossed text is removed to simplify the mesh.

After the preparation of the geometry is finished, the modal analysis model is created in Ansys Mechanical. The created geometry is automatically imported, excluding suppressed components. If variations of component selection need to be considered, all necessary components should be imported and suppressed individually in Ansys Mechanical. In the case of the VFD simulation, the base jig is imported into Ansys Mechanical but later suppressed.

The material properties of all the components in the model are added to the engineering data section of the modal analysis in the Ansys Workbench project. The exact material properties for some of the components such as the plastic casing and choke aluminum are specified. In addition, approximate properties for materials such as steel and copper are provided. The properties of the materials are presented in Table 1. The total mass of the VFD is approximately 5 kilograms.

Table 1. The materials and material properties used in the creation of the model.

Material	Density (kg/m^3)	Young's Modulus (Pa)	Poisson's Ratio (Pa)	Bulk Modulus (Pa)	Shear modulus (Pa)
Steel	7850	$2 \cdot 10^{11}$	0.3	$1.667 \cdot 10^{11}$	$7.69 \cdot 10^{10}$
Copper	8942	$1.26 \cdot 10^{11}$	0.345	$1.355 \cdot 10^{11}$	$4.684 \cdot 10^{10}$
Aluminum alloy, 6061, T6	2713	$6.904 \cdot 10^{10}$	0.33	$6.760 \cdot 10^{10}$	$2.595 \cdot 10^{10}$
PCB laminate, Epoxy / Glass fiber	1944	$2.437 \cdot 10^{10}$	0.1649	1.212e10	$1.046 \cdot 10^{10}$
Plastic, PC	1160	$2.303 \cdot 10^{9}$	0.4002	$3.846 \cdot 10^{9}$	$8.224 \cdot 10^{8}$
Plastic, PC+GF10	1250	$3.8 \cdot 10^{9}$	0.36	$4.524 \cdot 10^{9}$	$1.40 \cdot 10^{9}$

The mechanical properties of a printed circuit board (PCB) can vary highly based on the layout, material selection, and differing metal layering. Complex and small components of a PCB increase the difficulty in accurate modeling of the mechanical properties. Modeling of basic mechanical properties and behavior of a PCB does not require such a detailed model. (Lee et al. 2008, p. 1837.) In the case of modeling the mechanical properties of the whole variable frequency drive, sufficient simplification can be used to decrease the computational load with an acceptable level of accuracy.

Complicated components and assemblies in terms of detail, which do not possess significant structural importance, are modeled as distributed masses. These distributed masses are attached to their respective surfaces on which the original component would be located. An example of this is the front control panel of the VFD which includes high levels of detail while not acting as a structural member.

The bolts and screws in the VFD assembly are modeled as beam connectors. Beam connectors are structural elements that are used to carry a bending load from different bodies to another. The beam element is made using the previously created named selections for screws and bolts. Each beam element requires two connection geometries and a given diameter. The connection points are selected as the arcs at each end of the bolt location. An example of a beam connection with the geometry highlighted can be seen in Figure 15. The bolt elements are not used in cases where one bolt connects multiple components as these connections are done using fixed joints. Additionally, fixed joints are used in cases where the simulation is found to have trouble calculating using the beam elements.

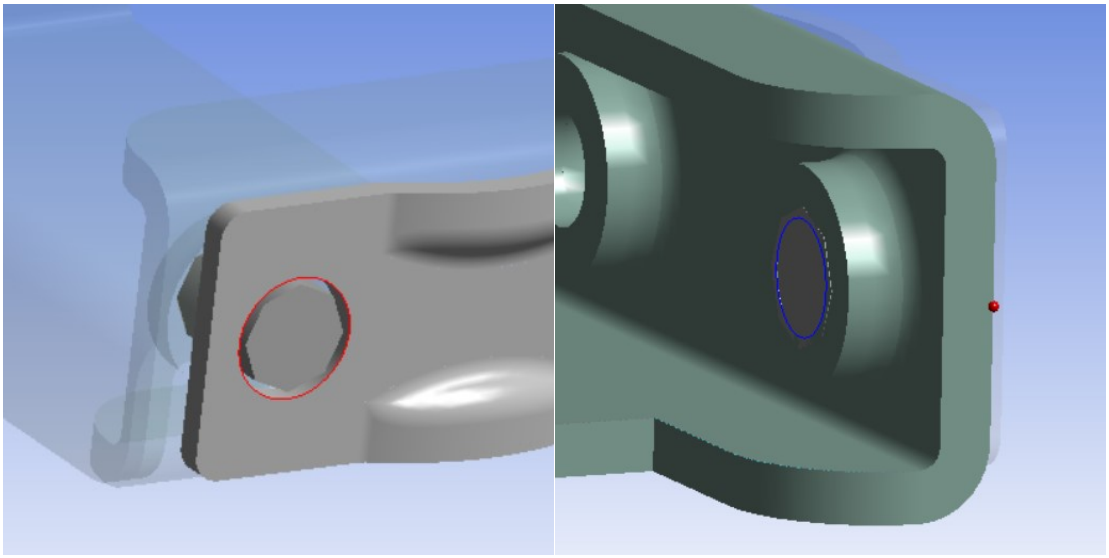

Figure 15. A beam joint with the reference geometries visible. The left side contains the reference scope and the right side contains the mobile scope.

Connecting different components together in subassemblies is done using joint connections and contacts. The fixed joint is created by specifying the joint type as “fixed joint”, which restricts movement in all six degrees of freedom. The scope of the joint is determined by selecting a feature for each component of the joint. In the case of PCBs, for example multiple components can be selected for the reference scope of the joint. The clip connector plastic casing joints are modeled as contacts at the touching edges of the clip connector and casing. Fixed supports are used to create the boundary conditions for the structure. Each attachment point of the VFD is selected and fixed to the ground by selecting the body-ground mode. All the connection types presented above and the total number of them are listed in Table 2.

Table 2. List of all used connection types and the number of connections.

Connections	Fixed	Beam	Contact	Total
Number of connections	77	27	2	106

The boundary conditions of the system are modeled as fixed supports in each attachment hole of the casing. Additionally, the upper and lower edge of the back wall is fixed to simulate a more rigid attachment. The attachment holes are highlighted in Figure 16.

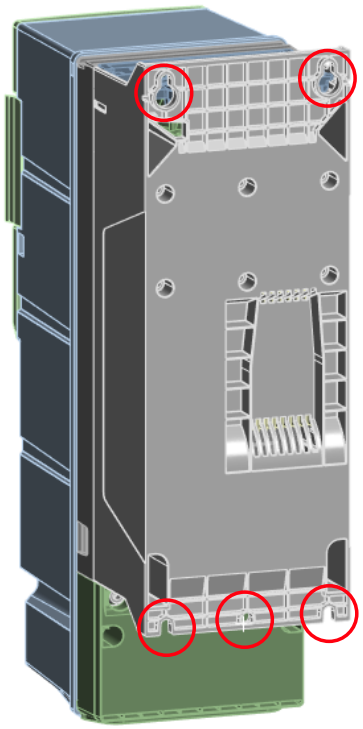

Figure 16. Locations of the attachment points.

The element order option in meshing defines the presence of mid-side nodes of elements. Quadratic elements include mid-side nodes in addition to edge nodes whereas linear elements do not. The two types of elements are presented in Figure 17, where the left side of the picture represents the linear element and the right side the quadratic element. Mid-side nodes increase the degree of freedom (DoF) of the quadratic element and subsequently increase the accuracy of the results. The computational load is also increased, and therefore linear elements are more often used in larger meshes. Quadratic elements are the best when used in applications requiring high element accuracy.

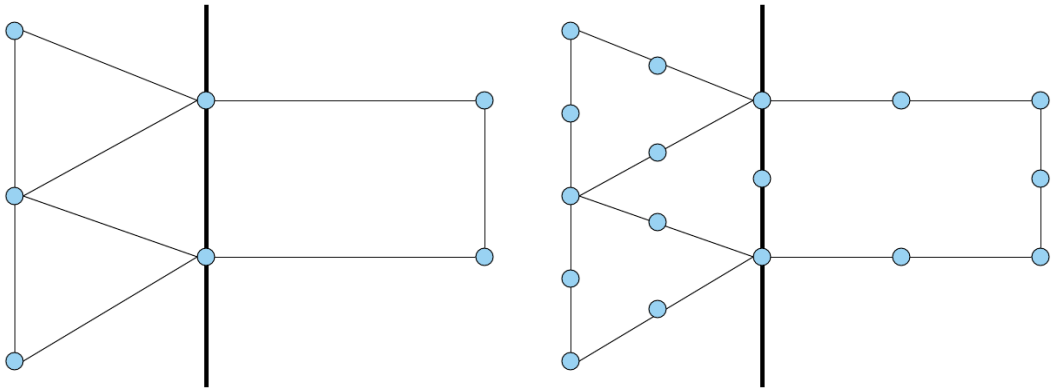

Figure 17. Example for linear (left) and quadratic (right) mesh elements (SpaceClaim 2024).

The vibration simulation consists of complex geometries that need to be modeled as 3D elements. Alternatively, the use of shell elements with specified thickness would be more computationally efficient but require simpler geometries and is therefore not applicable.

Element sizing is used to define the size of the generated mesh elements. The size of the elements highly influences the accuracy of the results but also increases computational load exponentially. The influence of the element size on the results starts to decrease exponentially once a converging mesh quality is achieved. Finding a good balance between accuracy and complexity is key to optimizing the performance of the model. Mesh size needs to be small enough to accurately depict the important geometry details (Kurowski 2016, p. 82). Ansys Mechanical has many different options for the physics preference used in the simulation. The main characteristic of a physics preference is whether it is linear or nonlinear. Mechanical physics preference was chosen as the modal analysis requires linear equations.

The physics preference also affects the mesh options available. By using mechanical physics preference, an adaptive mesh generation can be used, meaning element size is not fixed and can adapt to the geometry of objects. This allows for a more accurate depiction of complex geometries without the need to have small element sizes for larger features.

The main option for mesh creation is the global maximum element size which was selected to be 0.005 meters. Additionally, local sizing of mesh is used to determine local mesh sizes

for parts or faces. This is useful in a large assembly where the level of detail of components varies a lot.

Mesh creation can fail in complex geometries that cannot be represented using given mesh parameters. Meshing rarely is successful using default settings and configurations, especially in more complex geometries. (Kurowski 2016, p. 77.) The size of features and faces that get defeatured can be adjusted with a parameter that determines the smallest feature that will not get defeatured. This is a parameter that can be adjusted locally on components that fail to mesh with given global settings. Resolution is a meshing option that affects how coarse or fine the mesh is. Resolution is determined with a number, where a lower number indicates a coarser mesh. Transitioning is a parameter that determines how fast the size of elements can change. Faster transitioning allows for fewer total elements to be used.

On problematic components individual mesh sizes differing from the global mesh size need to be used. Depending on the number of failed features they can either be fixed by selecting the problematic faces or by selecting the entire component.

The generated mesh of the variable frequency drive can be seen in Figure 18. The picture shows the product after generating the mesh with the previously specified mesh parameters. The size of the generated mesh was 1939388 nodes and 1001857 elements.

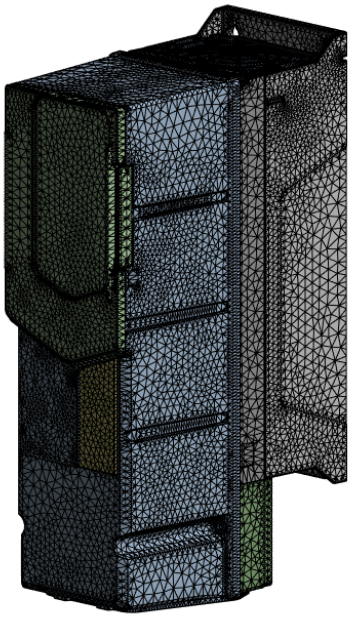

Figure 18. Generated mesh of the variable frequency drive.

Figure 19 presents the before and after of a mesh of simplified and untouched versions of a component. The left side shows the untouched and the right side the simplified mesh. The decreased number of elements is visually noticeable.

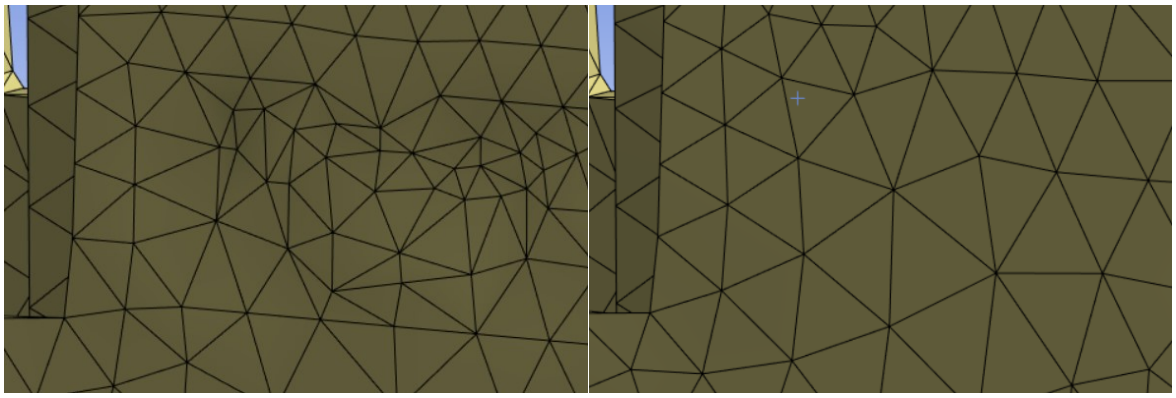

Figure 19. Example of untouched (left) and simplified (right) mesh of a component.

The project schematic of the analysis is presented in Figure 20. Modal analysis is used as the basis of the project. The engineering data, geometry, and model are shared with all the other analyses. The solution of the modal analysis is used in the setup of each harmonic analysis independently.

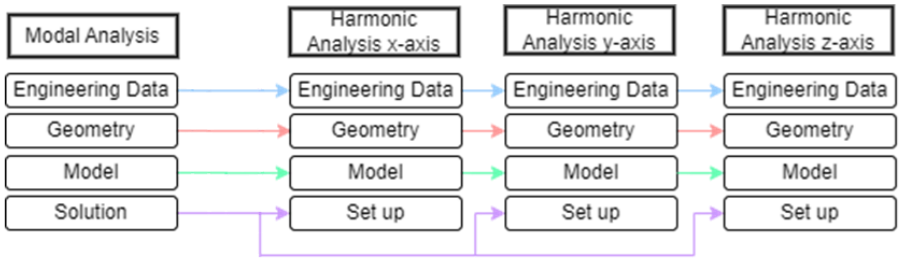

Figure 20. Project schematic. The relations of data flow between modal analysis, harmonic analysis, and endurance tests for each axis are displayed.

3.4 Modal analysis

Modal analysis determines the natural frequencies and mode shapes of an object. Results of the modal analysis can also be used in further analyses such as the harmonic response analysis.

The modal analysis is conducted using the structural modal analysis type in Ansys Mechanical. The theory of how the modal analysis is conducted in the FEA is presented in chapter 2.1. The case studies an MDoF undamped modal analysis for the VFD. The equation of motion is calculated for each individual mode.

According to IEC 60068-2-6 (2007, Annex C, p. 36), the frequency range of an environmental vibration test can be selected from the standard table C.2 based on the use specific use case. Amplitude range for an application in general industrial use can be tested with a frequency range of 10 Hz to 150 Hz.

The settings of the modal analysis determine the scope of the calculations. Only the frequencies within the range of 0 Hz to 200 Hz are studied. This range contains all necessary natural frequencies that would fall inside the range of 10 Hz to 150 Hz as previously determined. Additionally, the maximum number of modes to find is set to 100 to make sure all modes are included. Missing modes that are not inside the 10 Hz to 150 Hz range would affect the value and amplitude of the highest natural frequencies. Modes after 200 Hz are not considered as their effect on the system would be negligible.

The accuracy of the natural frequencies compared to the experimental results is evaluated by calculating the percentage error between the corresponding natural frequencies. The error is calculated according to the following equation (Könözsy 2020, p. 431-432):

$$\text{Frequency Error} = \frac{\left|f_{FEA} - f_{experimental}\right|}{f_{experimental}} \cdot 100\% \tag{13}$$

This equation calculates the absolute error of the FEA relative to the experimental results and is expressed as a percentage. The absolute relative error represents the percentage error if the experimental results are considered accurate. (Könözsy 2020, p. 431-432.)

3.5 Harmonic response

Unlike in the modal analysis, the harmonic response analysis uses a damping ratio. A global damping ratio is an experimental value that represents the percentage of critical damping. Obtaining accurate damping ratios through calculations is very difficult. If experimental testing cannot be used to determine the damping ratio, estimates should be used. Similar objects often have similar damping ratios. Estimates that will be used in the simulation of the VFD are between 1 and 5 percent. Multiple damping ratios are used to determine which is the most accurate at representing the damping behavior of the system. The length of the testing for a sweep from 10 Hz to 150 Hz with the speed of 1 octave per minute can be calculated according to the following equation:

$$\log_2 \frac{150}{10} \approx 3.91 \text{min} \tag{14}$$

The harmonic response uses the modal environment calculated in the earlier step of modal analysis. The analysis settings of the harmonic response are used to limit the calculated frequency range from 10 Hz to 150 Hz. The solution interval option determines the resolution of the result data. Increasing the resolution increases the compute time of the analysis. According to IEC 60068-2-6 (2007, p. 12), the sweeping rate for environmental vibration testing is 1 octave per minute.

Considering that a measurement is done once each second, the amount of measurement points can be calculated $60 \times 3.91 \approx 235$. A minimum of 235 interval points is required for an accurate representation of the testing parameters. For the final run of the analysis, the solution interval is increased to 250 to provide accurate and detailed data for the resulting frequency response plot.

The analysis uses mode superposition as the solution method, the theory of which is covered in chapter 2.1. Acceleration to the system is introduced as base excitation using tabular data. Base excitation is determined to affect the fixed boundary conditions of the VFD. The magnitude-phase testing data determines the acceleration load on the system. The used base

excitation data is presented in Figure 21. The figure uses an approximation of gravitational constant g that equals 10 $\frac{m}{s^2}$. Each analysis is plotted in the same logarithmic scale.

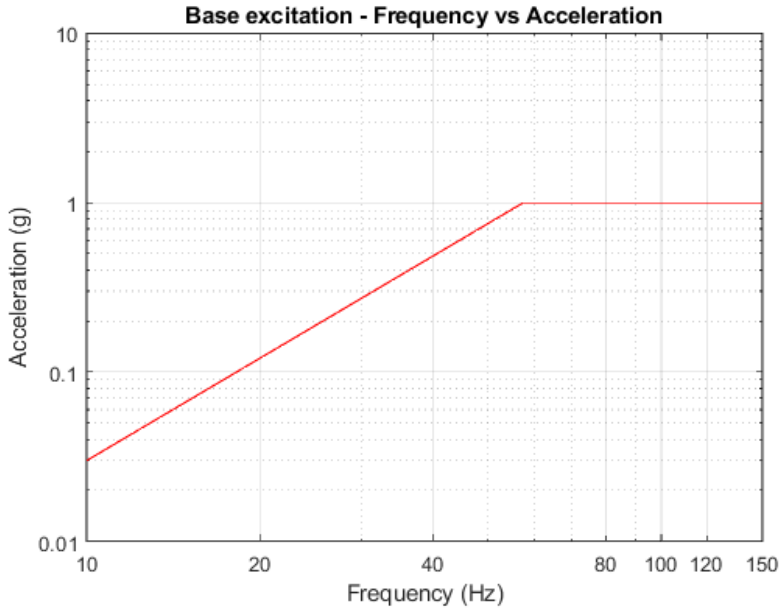

Figure 21. Frequency (g) – acceleration (Hz) plot of the base excitation data.

The frequency response can be calculated for a single axis at a time, so the harmonic analysis is done multiple times totaling three analyses, one for each axis. The peaks of the frequency response plots are collected and compared to the peaks of the experimental results, the error of which is calculated according to the following equation (Könözsy 2020, p. 431-432):

$$\text{Acceleration Error} = \frac{\left|g_{FEA} - g_{experimental}\right|}{g_{experimental}} \cdot 100\% \qquad (15)$$

where acceleration *g* represents either simulation or experimental acceleration peak. The error is individually calculated for each axis relative to the experimental results.

The frequency response is measured at a specific measurement point in the VFD. The location of the sensor in the experimental testing is seen in Figure 22. The measurement point of the simulation is visible in Figure 23.

Figure 22. Experimental testing set up with attached measurement points.

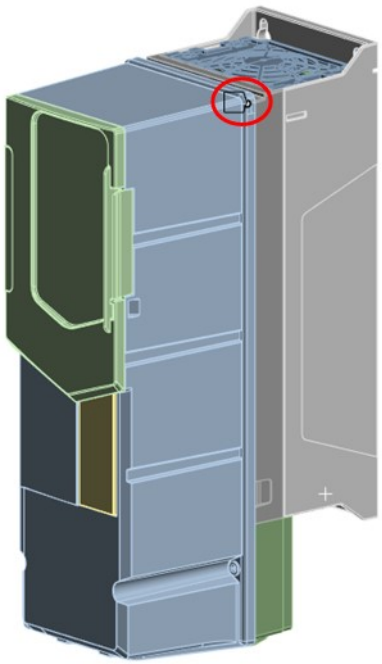

Figure 23. Location of the measurement point in the simulation.

3.6 Sensitivity analysis

A sensitivity analysis is conducted to evaluate the effects simulation parameters have on the results. This includes five simulation parameters and methods which affect the results, which include measurement locations, boundary condition configurations, mesh sizes, damping ratios and jig introduction.

Multiple measurement points are used to determine how much an inaccurate estimation of the actual location of the sensor affects the results. The location with the best correspondence is selected. All the measurement points, including the original one, are shown in Figure 24. The measurement points are labeled from A to F as seen in the figure. The corresponding measurement point abbreviations of the labels used in the result plotting are presented in Table 3.

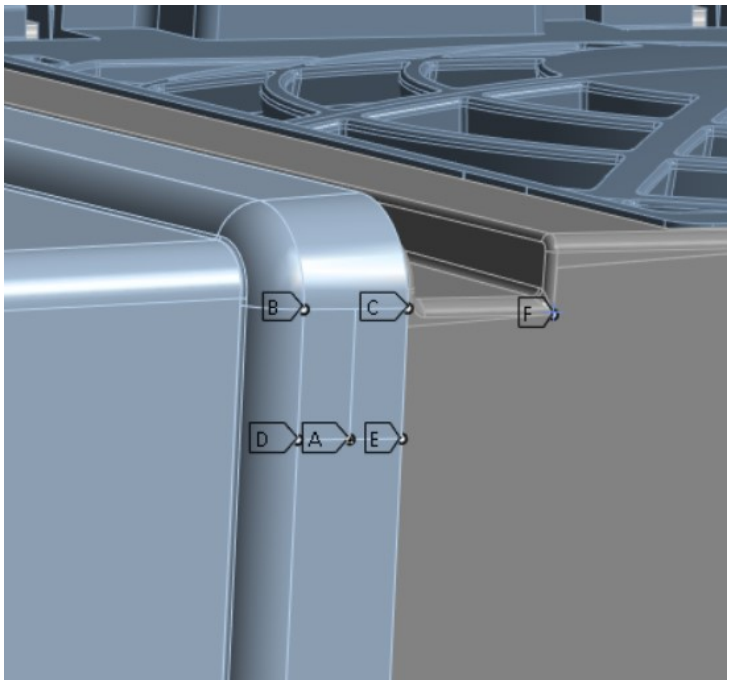

Figure 24. Locations of the additional measurement points near the original estimation.

Table 3. shows the corresponding name of each measurement point.

Simulation measurement point	A	B	C	D	E	F
Equivalent abbreviation in results	MP1	MP2	MP3	MP4	MP5	MP6

The effect different boundary conditions have on the results is evaluated. The original boundary condition BC1 consists of fixed attachments in all five mounting holes and fixed upper and lower edge of the back wall. Additionally, three other configurations are used to evaluate the effect and accuracy of the different modeled boundary conditions. Boundary condition BC2 consists of fixed attachment points at the five mounting holes of the VFD. Boundary condition BC3 similarly uses the attachment points, but only in the four main mounting holes. Lastly, the entire back wall of the VFD is fixed to simulate a fully rigid mount in BC4.

The mesh size is also one of the main factors that can affect the results of the simulation. The previously presented mesh parameters cannot all be evaluated. The resolution parameter is used to change the fineness of the mesh as this offers a simple parameter change that significantly affects the total size of the mesh. The amount of mesh elements is also listed to represent the size of the mesh.

The effect of modal damping ratios is presented by calculating the frequency response of multiple ratios. The selected damping ratios are within the range of 1 percent to 3 percent with an incremental increase of 1 percent between results, totaling 3 measurements.

Lastly, the significance of introducing a mounting rig is measured. The vibration characteristics of a jig are measured by calculating the results of the modal analysis with and without one and presenting the percentage difference in natural frequencies. The introduction of the jig is presented in Figure 25.

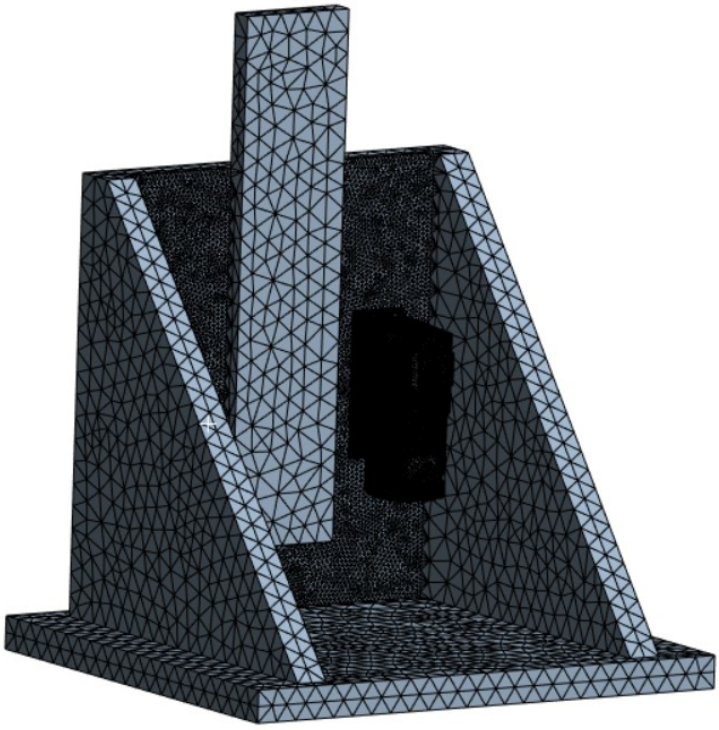

Figure 25. Mesh of the VFD, including the jig.

Figure 25 shows the mesh of the VFD when the jig is introduced. Unlike in the experimental set up, the other machines are not included in the simulation. The mesh element size of the VFD is much smaller which is why it is difficult to see in the figure.

3.7 Result post-processing

To improve the efficiency of the model, only necessary solution results are saved. This improves the execution time by limiting the size of the result files. The results of the frequency response analysis are presented on a logarithmic scale, where vertical axis utilizes a base-10 scale and horizontal axis utilizes a base-2 scale. The results are plotted using a MATLAB program and combined with the experimental data for comparison of results.

3.8 Simulation validation and reliability

Validation of the results is critical to ensuring that the simulation is representative of the actual system. The validation of the simulation is achieved by critically evaluating the results, such as natural frequencies and maximum amplitudes, in comparison to the experimental results. In addition, the results are compared to different configurations and parameter values in the sensitivity analysis. This is used to determine that the results are reliable, and possible anomalies can be detected. The simulation instability is discussed and the reliability of the used methods is evaluated.

4 Results

This chapter presents the results of the environmental vibration simulation. First, the results of the modal analysis are presented using the initial model. The resulting deformation of each mode is briefly inspected. The frequency response plots are presented by comparing to the existing experimental data in each axis, which was detailed in chapter 3.1. The results of each harmonic response plot are briefly explained and analyzed.

The results of the sensitivity analysis are presented using the initial settings and changing the respective parameters independently. The resulting natural frequencies and frequency response plots are presented. The initial analysis is done on each sensitivity analysis parameter.

4.1 Modal analysis

The natural frequencies obtained from the initial modal analysis are presented in Table 4. The natural frequency of the first five mode shapes is shown in Hz.

Table 4. Natural frequencies of the first six mode shapes.

Mode	1	2	3	4	5
Natural frequency (Hz)	57.1	108.1	123.1	132.5	149.6

In addition to the natural frequencies, the deformation patterns for the first five modes were inspected. The visual representation of the deformation is not to scale and is not to be used to measure the actual deformations, but rather to be used in visual analysis of the accuracy and behavior of the results. The visual inspection showed that the first mode mainly affects the entire system and presents in a wave deformation in the y-direction, which increases the further from the boundary conditions they are. Higher modes present more local deformation that is focused on the inner casing parts and the PCBs.

4.2 Harmonic response

The initial harmonic response results are displayed as frequency–acceleration plots for each axis. The x, y, and z-axis acceleration plots are presented in Figures 26, 27, and 28. Each plot displays the acceleration in the vertical axis and frequency in the horizontal axis. The plots use a logarithmic scale of base-10 and base-2 for the vertical axis and horizontal axis, respectively.

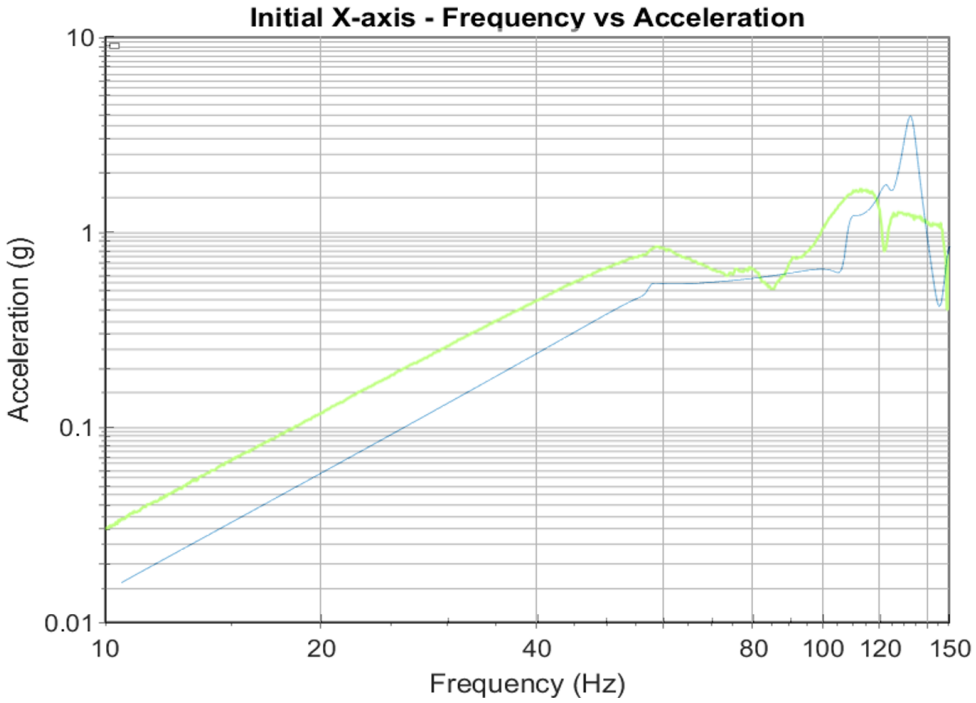

Figure 26. The frequency response of the simulation and the experimental results in the x-axis. Blue color represents the simulation data and green represents the experimental data.

The x-axis results shown in Figure 26 appear to loosely correlate to the experimental results. The main difference is that the base excitation does not seem to fully translate to the simulation body. The amplitude is slightly lower than the experimental results. The peak at 132.5 Hz shows a significantly larger acceleration magnitude peak than the experimental results. The peaks are also not at the same natural frequencies as the main peak in the experimental results is at 117 Hz. After the peak, the acceleration amplitude increases in the simulation, but the acceleration in the experimental result decreases. Overall, the correlation

between the peak magnitudes is not entirely accurate in the direction of the x-axis. The simulation natural frequency at the peak magnitude is higher than in the experimental results.

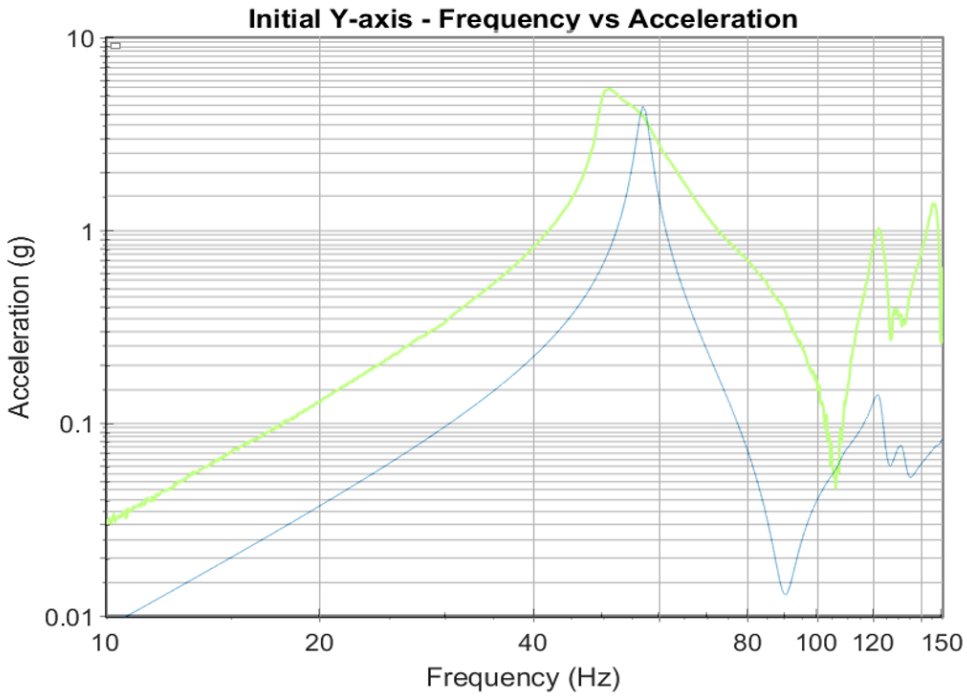

Figure 27. The frequency response of the simulation and the experimental results in the y-axis. Blue color represents the simulation data and green represents the experimental data.

The y-axis results shown in Figure 27 show some similarities at the first natural frequency. The magnitude of the main peak at the lowest natural frequency shows some correlation to the experimental results. Higher natural frequencies begin to show inconsistencies between the two results. The higher natural frequencies seem to correlate, but the magnitude of the higher peaks in the simulation is also much lower than in the experimental results. The results in the y-axis show that while the correlation between the lowest natural frequency is present, the magnitude of the acceleration is slightly lower.

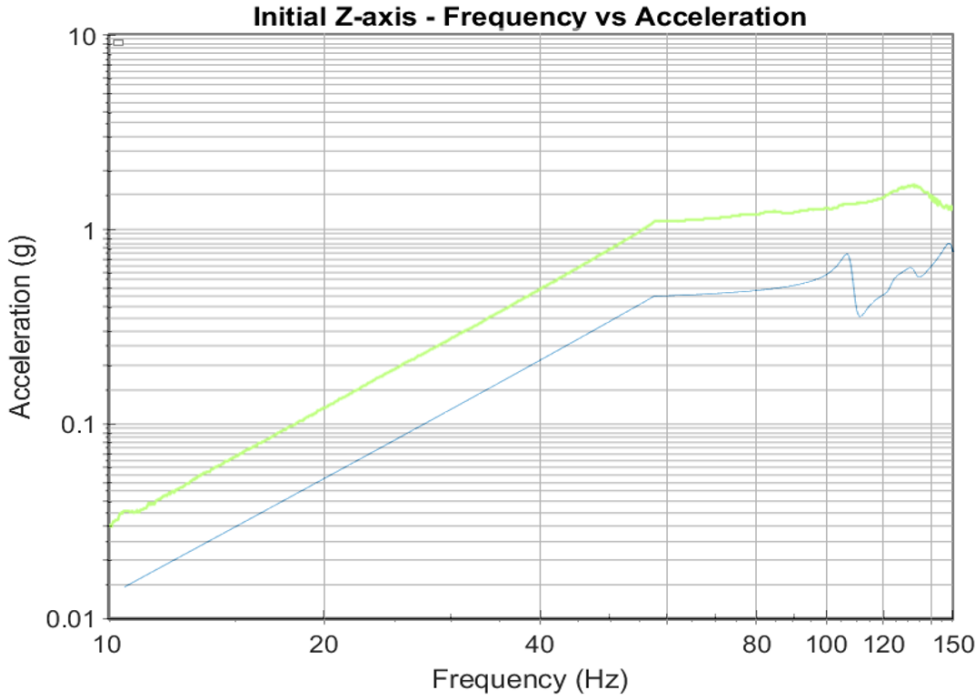

Figure 28. The frequency response of the simulation and the experimental results in the z-axis. Blue color represents the simulation data and green represents the experimental data.

The z-axis results shown in Figure 28 show a peak at 108 Hz, which is not present in the experimental results. Both experience a peak at 130 Hz, although the amplitude of the acceleration in the simulation is significantly smaller. The amplitudes and natural frequencies do not correlate well with the experimental results.

4.3 Frequency and acceleration error

Natural frequencies can be estimated from the harmonic response plots. The peaks can be measured for both the acceleration and frequency. The collected data can be used to calculate the error between the acceleration of the two methods. Equation 13 is used for calculating percentage error and is presented in chapter 3.4. Table 5 presents the percentage error of simulation results compared to the experimental results at the natural frequencies of the system.

Table 5. Natural frequencies of simulation and experimental results and the percentage error between them.

Mode	FEA – Natural frequency (Hz)	Experimental – Natural frequency (Hz)	Error (%)
1	57.1	51	12.0
2	108.1	113	-4.3
3	123.1	123	0.1
4	132.5	132.5	0
5	149.6	145	3.2

The highest acceleration peak in each axis of the harmonic response plots is presented in Table 6. The acceleration error between the simulation results and experimental results is calculated using equation 15 presented in chapter 3.5.

Table 6. Acceleration results in comparison between simulation and experimental results at similar natural frequencies.

Acceleration axis	Simulation – acceleration (g)	Experimental – Acceleration (g)	Error (g)	Absolute error (%)
X	3.9	1.7	2.2	129.4
Y	4.4	5.5	-1.1	20.0
Z	0.85	1.7	-0.85	50.0

The error between natural frequencies is calculated in Table 5. The error represents the accuracy to which the simulation system is capable of accurately predicting the natural frequencies. Knowing natural frequencies can be critical knowledge when the likely range of vibration is known. If significant natural frequencies coincide with the experienced vibration range, changes to the product might be needed. The table shows that the lowest mode shows the most inaccurate results of 12% error. Higher modes all show an absolute error lower than 5%, which suggests a good correlation.

The error of experimental and simulation acceleration results at natural frequencies shown in Table 6 indicates how well peak accelerations correlate to true measurements. A larger error indicates that the simulation does not match the resulting stresses of the true system. The negative error would indicate that the simulated system experiences smaller than true

stresses and the positive error would show stresses too large. Additionally, the absolute percentage error can be seen, which can better display the magnitude of the difference between the results. Comparing the maximum acceleration amplitudes in Table 6 of each axis shows that significant inaccuracy is present in all axes, especially in the x-axis.

4.4 Results of the sensitivity analysis

In this chapter, the results conducted according to the previously detailed sensitivity analysis are presented. The frequency response plot of six different measurement locations is presented in Figure 29. The locations are according to Figure 24 presented earlier.

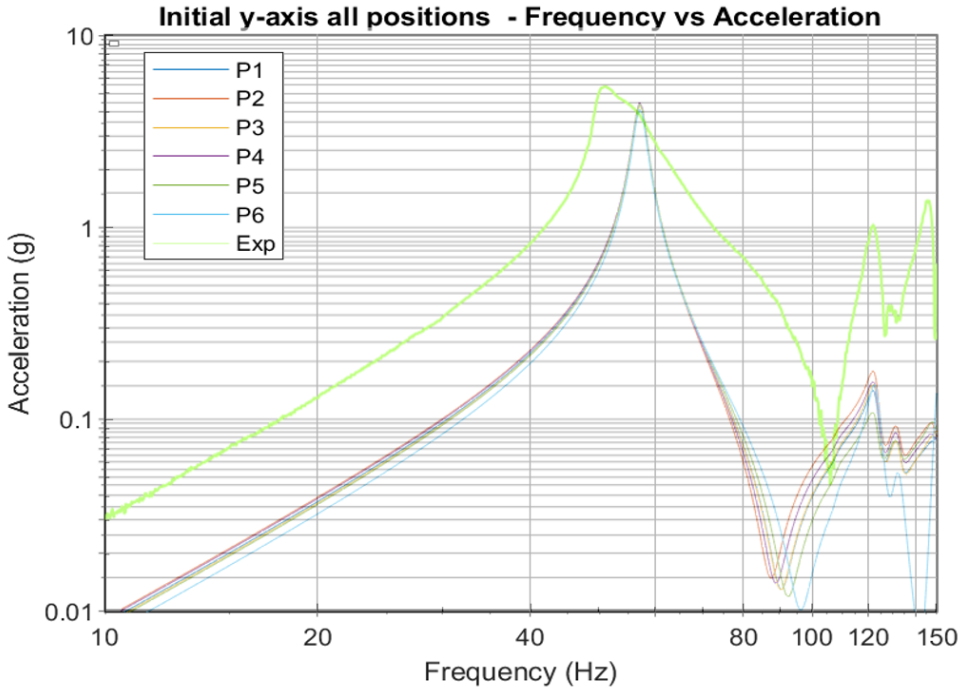

Figure 29. The frequency response of the simulation in the y-axis for six different approximate positions. The corresponding positions are displayed in Figure 24 and abbreviations are explained in Table 3.

The harmonic response plot in Figure 29 shows that the measurement location does not affect the natural frequencies of the system. The amplitudes are affected by measurement points as the deformations are not uniform across the whole body of the system.

Results show that the lowest mode has nearly identical amplitude in each measurement position. This can be explained as the movement of the first mode is a swaying movement from side to side in the y-axis, which is seen from the deformation animation from the modal analysis. Movement is more significant the further away the measurement location is from the fixing wall. As the measurement locations are relatively close to each other in comparison to the entire body, the effect on amplitude is minor.

The position does affect the amplitudes at the higher natural frequency range. The modal analysis shows that the deformations of modes 2-5 are more pronounced in the internal components of the system. These deformations cause more variation in the results of each individual measurement point.

Location P6 is shown to have the lowest valley at approximately 96 Hz, whereas P2 has the lowest valley at approximately 87 Hz. As the valley in the experimental results is approximately at 106 Hz, location P6 provides the closest result. The results show a trend that the closer to the fixing wall the measurement point is located the higher the frequency for the lowest valley is. P6 shows a significant valley at the highest natural frequency, where none of the other locations did.

All locations P1 to P5 were situated in the same casing part whereas P6 was further back in the main frame of the product. The definition of the joints and contacts between these components is likely to explain the large difference between the results. The load distribution is more uniform within a single solid part than across two connected parts. This also shows that the higher natural frequencies are much more dependent on the exact location of the measurement. For the most accurate comparison between the experimental results and the simulation results, a properly documented location of the sensor is critical.

The frequency at which the lowest valley occurs can vary up to 10 Hz between locations, which is a significant variation. In conclusion, the amplitudes at the lowest natural frequency are not as sensitive as the higher frequencies.

Multiple different boundary conditions were applied, and the natural frequencies and frequency response plots were presented. The boundary conditions are according to the previously detailed descriptions in chapter 3.6. In Figure 30 the frequency response plot in the y-axis of the 4 different boundary conditions are presented. Table 7 presents the natural frequencies of the first five modes for each boundary condition.

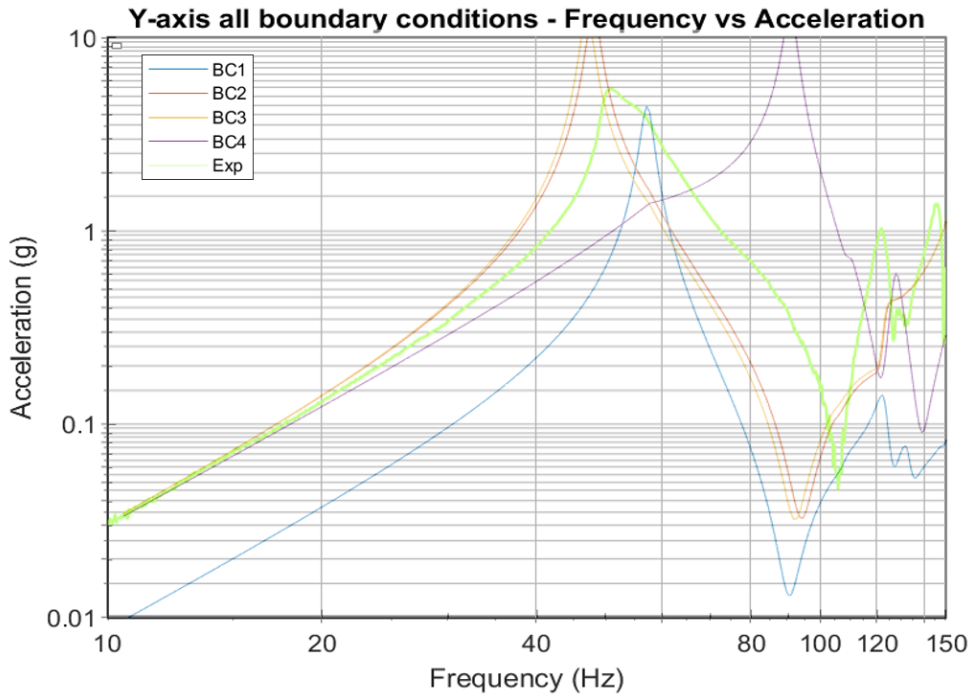

Figure 30. The frequency response of the simulation in the y-axis for 4 different boundary condition cases.

Table 7. Natural frequencies of different boundary conditions.

Modes	Holes, top and bottom edge (BC1)	Five mounting holes (BC2)	Four mounting holes Holes (BC3)	Entire back (BC4)
1	57.1	48.0	47.0	90.8
2	108.1	105.1	104.9	109.7
3	123.1	117.8	117.4	127.5
4	132.5	123.2	122.9	143.0
5	149.25	149.3	148.8	151.8

The harmonic analysis results of the four different boundary conditions shown in Figure 30, show that the initial boundary condition (BC1), where five mounting holes and the lower and upper edges are fixed to the back of the drive, was flawed. This can be seen most notably by how the initial boundary condition (BC1) has much lower amplitudes across the entire frequency spectrum. This configuration is shown to be inconsistent with the experimental results and the other boundary conditions.

The initially selected damping ratio of 2% results in amplitudes for BC2, BC3, and BC4 that are much higher than seen in BC1 or the experimental results. This suggests that the damping of the system is higher than the initially used 2%.

The other 3 boundary condition configurations (BC2, BC3, BC4), while having much larger maximum amplitudes, show better alignment to the amplitudes of the experimental results across the entire frequency spectrum. This is significant in the frequencies between 10 Hz and the first natural frequency at approximately 52 Hz, where all other boundary conditions and the experimental data closely follow the amplitudes of the base excitation.

Boundary condition with the fully constraint back wall (BC4) makes the system too stiff in comparison to the experimental results. The lowest mode being at 90 Hz, instead of approximately 52 Hz in the experimental results, suggests that the simulation is not accurately representing the actual behavior.

Boundary conditions using the five or four mounting holes (BC2, BC3) as the fixed boundary conditions show similar results. Fixing from all five holes shows slightly larger stiffness resulting in slightly higher natural frequencies. In comparison to BC4 the lowest natural frequencies of the two boundary conditions are much closer to the experimental results, making them the more accurate representations of the actual system.

The natural frequencies, using four different mesh resolution settings, are presented in Table 8. The first five modes are presented in addition to the node and element count of the mesh.

Table 8. Natural frequencies using different mesh resolutions and mesh sizes.

Result	Resolution 0	Resolution 1	Resolution 2	Resolution 3
Mode 1.	66.8	57.1	66.4	66.4
Mode 2.	110.6	108.1	108.3	108.3
Mode 3.	123.9	123.1	122.4	122.1
Mode 4.	132.8	132.5	132.0	131.2
Mode 5.	152.7	149.25	148.33	148.6
Nodes	1756043	1942345	2083206	2433008
Elements	893262	1003585	1106041	1337047

Table 8 shows the effect of increasing the mesh resolution parameter has on the mesh size of the system. Increasing the mesh resolution parameter increases the size of the mesh, and subsequently reducing it lowers the mesh size. The results of the modal analysis show that resolutions 0, 2, and 3 show similar natural frequencies. Using resolution 1 resulted in significantly different results which was unexpected behavior.

This behavior could be caused by low-quality mesh or some other instabilities in executing the numerical calculations. This occurrence could be specific to the used boundary conditions and parameters, and different configurations might not show the same inaccuracy.

Mesh resolution 0 shows more difference when compared to resolutions 2 and 3, suggesting that the adequate resolution to accurately depict the system is achieved using the higher mesh resolutions. The differences between 2 and 3 are minimal and the lower mesh size should be selected for more efficient calculations.

The frequency response plot in the y-axis for three damping ratios is plotted in Figure 31. The damping ratios were one, two, and three percent. The maximum amplitudes using each damping ratio are presented in Table 9.

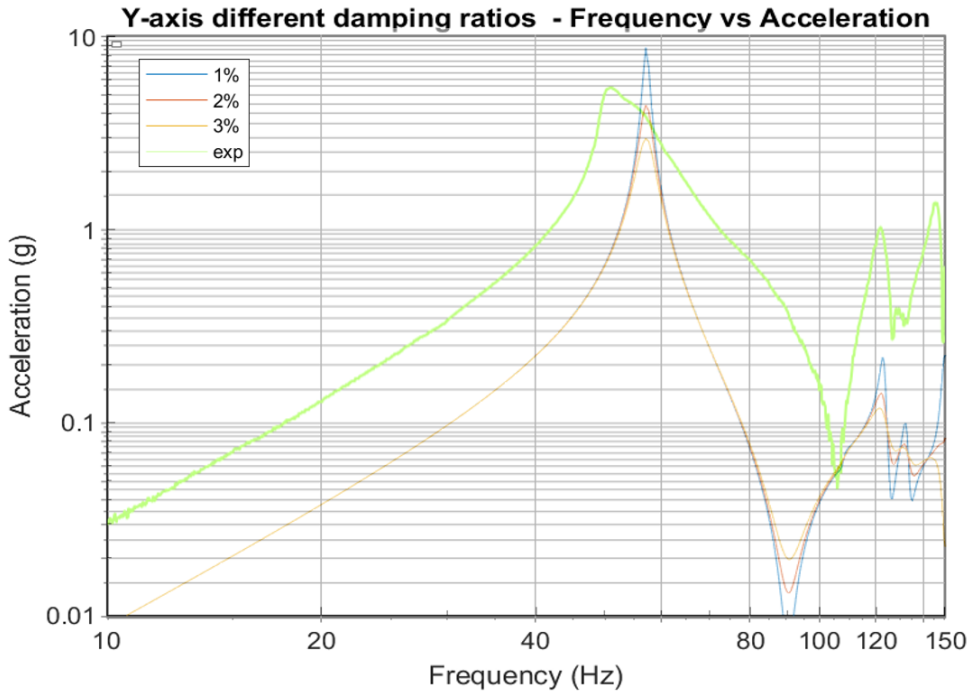

Figure 31. The frequency response of the simulation in the y-axis for three different damping ratios.

Table 9. Maximum amplitudes using different damping ratios

Damping ratio	1%	2%	3%
Max. amplitude (g)	8.75	4.43	2.97

Adjusting the damping ratio of the harmonic analysis expectedly resulted in lower spikes at each natural frequency. A higher damping ratio reduced the maximum and minimum amplitudes. In addition, the higher damping generally smoothened the results, which is noticeable especially in the higher natural frequencies. There is no effect on the natural frequencies of the system as the damping ratio is only used in the harmonic analysis and not applied when calculating the modal analysis.

Table 9 shows that increasing from 2% damping to 3% damping shows significantly different maximum amplitudes. Maximum amplitude at 2% damping is approximately 50% larger. When the main goal of the harmonic analysis is to accurately estimate the maximum amplitudes of the system, correctly estimated damping ratio is critical. The maximum amplitudes are the main concern for which the experimentation and simulation would be done. Maximum amplitude determines whether the drive passes the industrial environmental vibration test.

The drive has rubber gaskets between some of the main structural components to provide environmental protection. The gaskets are difficult to model and are therefore not included in the simulation. As rubber has a high damping ratio, the system's overall damping ratio would be higher if the gaskets were included in the simulation compared to a product without the rubber.

The effect of introducing a jig on the modal analysis is presented in Table 10. The results are compared to a comparable boundary condition of four fixed holes. The percentage difference with respect to the boundary condition (BC3) of the two configurations is presented in the table. Figure 32 presents the frequency response plot in y-direction with the introduction of the jig, 4-hole boundary condition and experimental results.

Table 10. Natural frequencies of different boundary conditions.

Modes	4 Holes (BC3)	4 Holes with base jig	Difference %
Mode 1.	47.0	47.0	0
Mode 2.	104.9	105.0	0.1
Mode 3.	117.4	117.4	0
Mode 4.	122.9	122.9	0
Mode 5.	148.8	148.8	0

Results of the modal analysis in Table 10 show an effectively identical result between the two configurations. Notably, the overall size of the mesh increases by approximately 4 percent when using a very rough mesh for the jig. Higher mesh density would exponentially increase the mesh size.

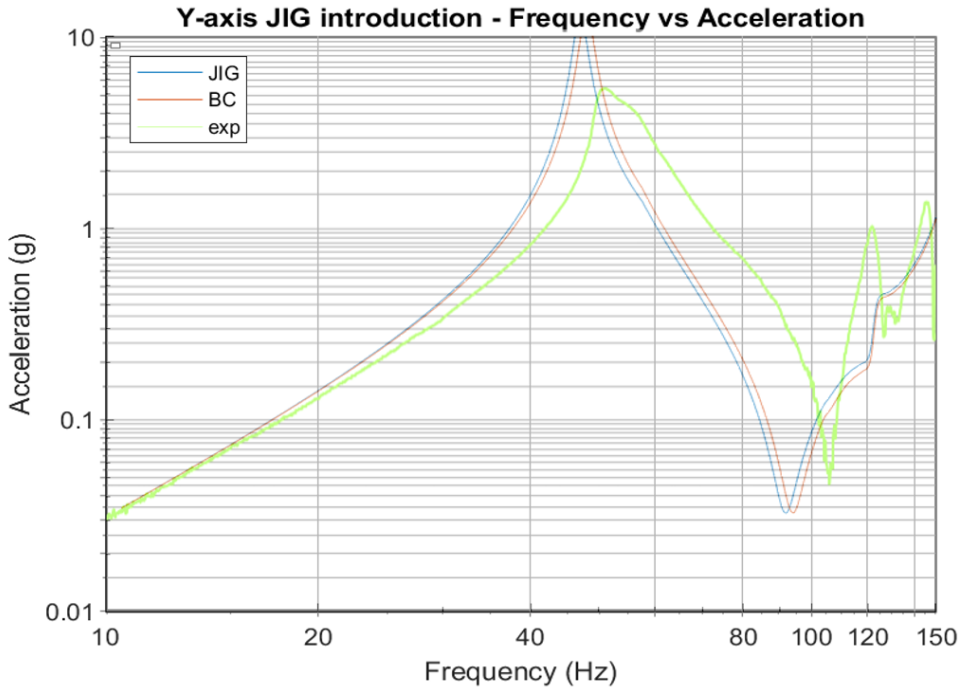

Figure 32. The frequency response of the simulation in the y-axis with the jig, 4-hole boundary condition and experimental results.

The maximum amplitudes in the frequency response plot were 13.4 g and 14.0 g, for the jig and boundary condition configuration, respectively. The results show an approximately 5

percent decrease in maximum amplitudes and slight decrease of 1 Hz for the location of the maximum amplitude.

Table 10 shows that the natural frequencies are effectively identical to similarly fixed boundary condition configuration. This shows that the size of the VFD, with a mass of approximately 5 kilograms, is very insignificant compared to the mass of the aluminum jig. The results of the frequency response plot showed an approximately 5 percent lower maximum amplitude when compared to the similar layout without the jig. This suggests that the damping characteristics of the system are affected by the jig, or the connection to it. The accuracy of this result is unclear as the used mesh was only locally dense, and much larger elements were used elsewhere. The total effect on mesh size was noted to be relatively small at only approximately 4 percent. Using a finer mesh was attempted but it resulted in a 50% increase in mesh size while increasing memory allocation requirements so much that the simulation could not be executed. The frequency response plot also showed a minor 1 Hz shift towards lower frequencies at the maximum amplitude frequency.

5 Analysis and discussion

In this chapter the results and initial analyses presented in the previous chapter are analyzed and used to answer the research questions of the thesis. Based on the initial results and sensitivity analysis, the final results are created. They are presented and used to analyze the success of the case study. Additionally, the shortcomings and limitations of the results are critically evaluated and discussed.

5.1 Analysis of the initial simulation results

The results of the initial simulation results showed that accurate modal analysis of natural frequencies could be achieved using the initial parameter selection. The results of the harmonic analysis had also a similar maximum amplitude to the experimental results. However, further analysis of the results showed the base excitation amplitudes were not correctly represented in the initial results. This results in skewed results which while somewhat accurate in terms of natural frequencies, fail to predict accurately the acceleration amplitudes of the higher natural frequencies. Higher frequencies tend to be less accurate and provide much less reliable results. Harmonic analysis was most accurate for the initial y-axis as it was the most affected by the lowest mode. Other axes and modes don’t have a good correlation to experimental results, which likely explains the inaccuracy of the results.

5.2 Analysis of the results of the sensitivity analysis

The results of the sensitivity analysis highlighted the variability of the results based on the selected parameter changes. The most sensitive parameters were shown to be the boundary condition and damping ratio. The importance of other parameters was also noted, but they were relatively minor in comparison, except for the mesh resolution parameter, which highlighted an anomaly in the simulation calculations. It was shown that the results differed from using both smaller and higher mesh resolution settings, which is not expected behavior.

The definition of the boundary conditions was most significant factor in determining the natural frequencies of the modal analysis. Boundary conditions affected the amplitudes of

the system less, expect in the case of the initial boundary condition (BC1). The results highlighted how unlike other the other configurations, the original results did not follow the base excitation amplitudes correctly. This suggests that the boundary condition did not accurately transfer the base excitation.

The damping ratio of the initial result provided appropriate maximum amplitudes in the initial results. When using appropriate boundary conditions, the amplitudes increased and therefore the initial damping ratio was not accurate. The effect of single digit percentage change of the damping ratio was shown to be very significant. Increase resulted in the maximum amplitude being 50% higher. This shows that even a single percent increase of the damping ratio can determine whether the resulting amplitudes are within the acceptable range of the environmental testing standard.

The parameters of the sensitivity analysis were individually changed using the initial simulation results. This means that in each different parameter study the rest of the parameters stayed the same as in the initial simulation. The results of the sensitivity analysis do not directly point to the correct selection of a parameters as changing the value of one can affect all others. The results can be used to understand the model better for further optimization of the simulation.

5.3 Analysis of the final results

The final results of the case study are made using insights from the sensitivity analysis. The parameter values are selected to create results with the best correlation to the experimental results. Since changing multiple parameters can affect the results in unpredictable ways, some further iteration is needed.

The sensitivity analysis found that the initial boundary condition was incorrect, and it was changed to reflect an attachment where four of the mounting holes were fixed. The new boundary condition resulted in much higher amplitudes, which then was addressed by increasing the damping ratio to 5%. It was also shown that the mesh resolution setting of 1 was not consistent with other resolution settings. In the final results, the mesh resolution parameter was set to 2 to improve the result accuracy.

The final results were examined for all six measurement points and the best corresponding point was determined to be measurement point MP4 as it provided the best correlation with the experimental data. The selected parameters for the final simulation are presented in table 11.

Table 11. The final selection of parameters based on the sensitivity analysis.

Position	Boundary condition	Mesh resolution size	Damping ratio	Utilization of the jig
MP4	BC3	Resolution 2	5%	No

The natural frequencies of the final results are presented in Table 12. The table compares the simulation results to the experimental results, with the percentage error between them also presented. The natural frequencies are all within 6% of the experimental results in absolute terms. The first four modes have a negative error, while the fifth mode has a positive error. Considering that the experimental results also have a ±5% uncertainty, the scale of the error is within a reasonable range.

Table 12. Simulation and experimental result natural frequencies and percentage error between them.

Mode	FEA – Natural frequency (Hz)	Experimental – Natural frequency (Hz)	Error (%)
1	49.0	51.0	-3.9
2	106.9	113.0	-5.4
3	121.1	123.0	-1.5
4	125.4	132.5	-5.4
5	149.3	145.0	3.0

In Figures 33, 34, and 35 the final harmonic response plots of the case study are presented. In all figures the experimental results are represented by light green color and simulation results by blue color.

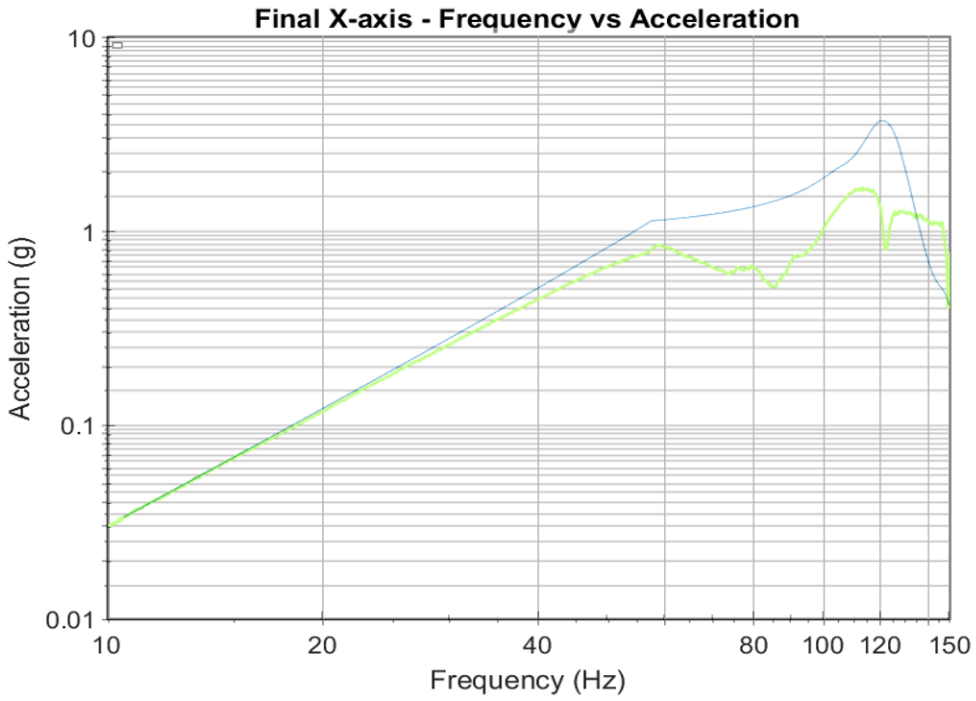

Figure 33. The frequency response of the simulation and the experimental results in the x-axis. Blue color represents the simulation data and green represents the experimental data.

Figure 33 shows the harmonic response of the system in the x-axis for both the final results and the experimental results. The plot shows that while the experimental results experience a valley at approximately 85 Hz, the simulation results show a steadily increasing curve. The maximum amplitude of the simulation results is nearly 3.5 g, while the experimental results show a maximum of approximately 1.6 g. This difference is significant and shows that the simulation in the x-axis is not entirely accurate. Both results have a decrease in the amplitude at the plot limit of 150 Hz.

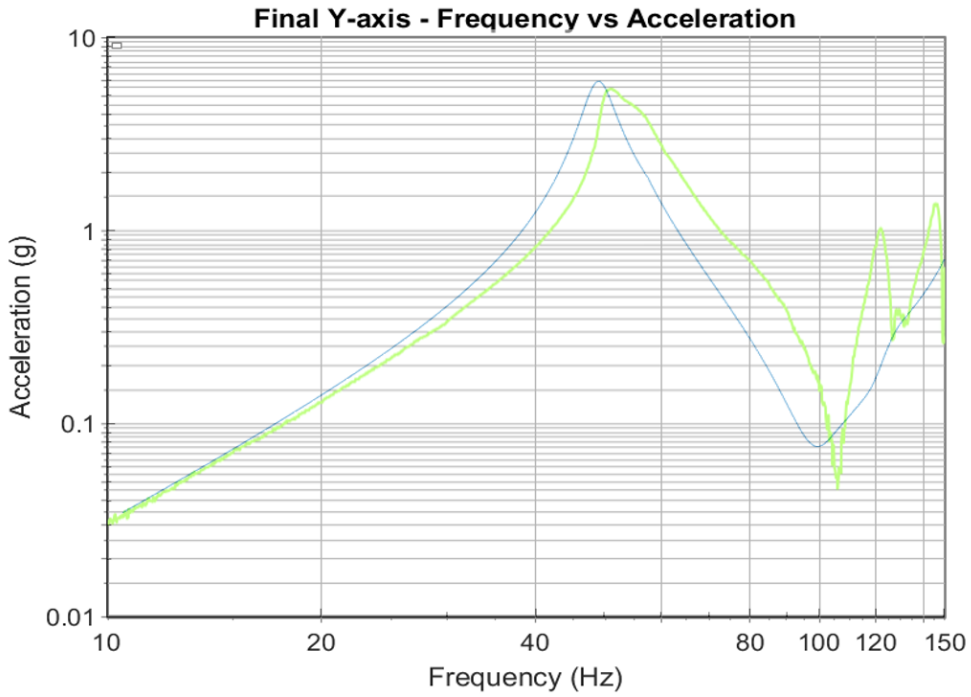

Figure 34. The frequency response of the simulation and the experimental results in the y-axis. Blue color represents the simulation data and green represents the experimental data.

Figure 34 shows the harmonic response of the system in the y-axis for both the final results and the experimental results. The plot shows a good correlation between the maximum amplitudes of the system. The maximum amplitudes are approximately 5 g and 4.5 g, for the simulation and experimental results, respectively. This results in an approximately 10% absolute error. Both results experience a valley at nearly 100 Hz, though the experimental results fall to a significantly higher amplitude of approximately 0.045 g, whereas the simulation falls to approximately 0.075 g. The simulation results show a much higher level of damping, which is most visible in the lack of sharp changes in amplitude such as in the experimental results. In comparison the simulation results are smooth, and changes are less drastic. Overall, the y-axis maximum amplitude and the overall trend of the amplitudes have a noticeable correlation.

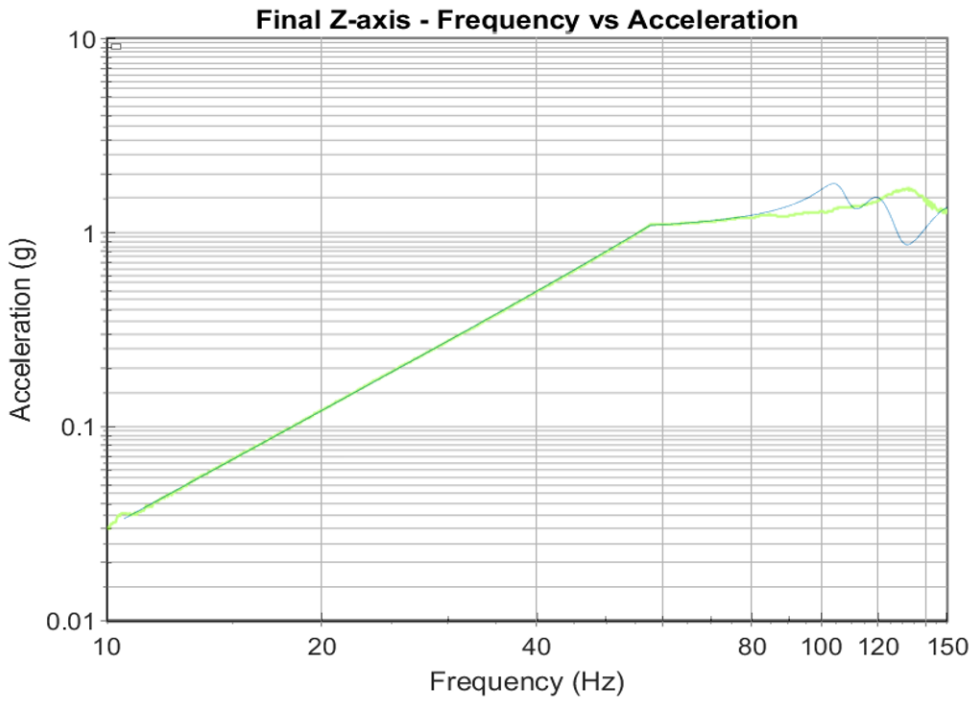

Figure 35. The frequency response of the simulation and the experimental results in the z-axis. Blue color represents the simulation data and green represents the experimental data.

Figure 35 shows the harmonic response of the system in the z-axis for both the final results and the experimental results. The maximum amplitudes of both results are similar, although at different natural frequencies. The peak in the experimental results happens at approximately 132.5 Hz, whereas the peak of the simulation results is at approximately 105 Hz. Additionally, when the maximum peak of the experimental result occurs, the simulation experiences a decrease in amplitude to approximately 0.9 g.

The representation of higher natural frequencies is less accurate in comparison to the smallest mode in all three axes. The lowest mode represents a swaying motion that involves the entire product. This makes it much easier to model and accurately represent. The higher modes have more local effects on the inner components of the system. This is likely one of the main reasons why it is more difficult to accurately represent them. Since the measurement happens in the outer part of the main frame, these inner deformations can cause inaccuracies in the results.

The x-axis had the largest difference in the maximum amplitude between simulation and experimental results. This suggests that some modelled components, such as the PCBs and

their plastic casings, do not accurately represent the true behavior especially when excited from the x-axis. This is likely due to more complex attachments between those components, such as plastic snaps.

The maximum amplitude the system experiences occurs in the y-axis direction and is the most important metric for standard approval. The peak occurs at the lowest natural frequency and the deformations in the lowest mode were found to affect the entire product. Fortunately, this makes it easier to model as the accuracy of the mode is not as dependent on the more complex and smaller components inside the case. This would suggest that in this case the modeling of maximum amplitudes is more accurate than the rest of the response.

5.4 Validity and reliability of the results

The validity of the simulation can be measured by evaluating the ability to represent the actual behavior of the system when experiencing sinusoidal environmental vibrations. The critical behaviors include damping, connections, material modeling, boundary conditions and system loading. Evaluation of the simulation results in comparison to experimental results adds to the validity of the simulation.

The modeling of damping was done using a universal damping ratio. This provides an easy approximation that assumes each component and material has uniform damping behavior. The materials used in the VFD vary greatly. The main parts are made of plastic which in this case is a mostly a simple material to model, however, one of the used plastic materials is a composite that uses fiberglass as a component that gives better structural properties.

Electrical components, such as PCBs, wires and individual components, are a mix of composites, metals and plastics. The accurate modeling of the electrical components is less important since most of them do not act as structural components. Most structurally significant electric components are the PCBs that are structurally connected to the rest of the product.

The glass fibers used in both the plastic parts and PCBs can make the material more direction-dependent in its structural behavior based on how the material settles during the molding or manufacturing process. This behavior is not considered in the simulation material

properties, and it could contribute to the system's overall vibration characteristics as it's used in main structural components.

Sheet metals are also used as structural components, and their modeling can be considered the most accurate out of all the materials. The model did not include the environmental proofing rubber gaskets which have a high damping ratio. This would increase the total damping of the system. Each material has its own damping ratio, but this behavior was not modelled in the simulation.

Creating accurate connections between components is one of the most difficult parts of modeling the VFD. Having 54 components requires approximately 106 connections. The bolted connections are easier to accurately model compared to plastic clip joints. Accurate modeling of the plastic clips would require sophisticated surface connections and would increase the complexity of the computation. The modeling process showed that joint type affects the results significantly. Overconstraint connections or loose components would dominate the vibration characteristics.

The literature review found mainly simulations of individual components or simple assemblies. This suggests that the difficulty in creating simulations for assemblies found in the case study is likely the reason why most studies focus on simulating on component-level.

The results showed that adjusting the boundary conditions has a large effect on the natural frequencies. This means that the boundary conditions are one of the most important factors in achieving accurate results. The chosen four-hole attachment boundary condition is likely to be accurate as the jig the VFD is attached to is very rigid. Modeling the joints as rigid means that it’s expected that the jig has minimal deformations.

In the literature review the importance of accurate boundary conditions was noted in multiple research papers. This further validates the findings of the case study by finding similar results from others in the field.

The results converging when increasing the mesh size affirms that the size of the mesh is not significantly limiting the model accuracy. The mesh quality should be checked for whether there is a high amount of poor-quality meshing.

The sensitivity analysis showed that certain parameters such as the damping ratio can have a large effect on the result. Accuracy in damping ratios is critical as one of the main goals of such vibration simulation is to find out the maximum amplitudes.

Comparing experimental results is critical in evaluating the validity of the results. This can be a problem when it would be very beneficial to conduct simulation testing before physical prototypes are made. Achieving validity of the results can therefore be difficult if experimental results are not available. Using data from similar products can provide guidance, but ultimately validity would come from experience.

Reliability is essential in ensuring a reproducible and stable process for simulation model creation. Reliability should cover both the model creation and model behavior. The unreliable model might give initially accurate results but could fail when trying different parameters or initial conditions.

The main goal of model creation description is to be able to recreate the results consistently. Accurate descriptions of the used model creation methods are critical to facilitating its recreation. Most steps are presented in the thesis, but the model creation does require individual skills from the model creator to interpret and fix problems that may arise during the process.

The reliability of the results highly relies on the assumption that the original experimental results are accurate. This is hard to verify afterwards, but knowledge of the quality of the experiments helps to identify its reliability. In this case, the experiments were conducted by a reputable laboratory specializing in vibration analysis which strengthened the trust in the results.

Bad mesh quality could cause failures in meshing or the result calculation. The initial mesh size at resolution setting 1 was shown to have possibly bad mesh quality as it differed significantly from the other resolution settings. This shows that the reliability of the simulation results improves by conducting a sensitivity analysis where these behaviors can then be detected. Sensitivity analysis can be used to reveal incorrect behavior. The import of the original 3D model caused many instabilities in the simulation. There were multiple faces that were not meshed properly, and these faces would then cause errors and crashes in both the model preparation software and analysis software. During the modeling process, it was found that bolt connections would cause instability in the simulation. Simplifying these

connections helped in achieving successful and more consistent results. While the simulations were running there was a significant risk of failure if the simulation machine was used for other purposes and in many cases the results file was corrupted. Frequent backups were needed to prevent losing all files relating to the simulations.

5.5 Limitations

The accuracy of the material properties used in the simulation is not fully accurate. Some of the components do not use the exact material properties but use similar generally available material properties. The inaccuracy in the material properties and the simplifications and reductions to the system affect the total weight of the system. This will clearly alter the results according to the difference between true and simulation weight.

Some inaccuracies between the simulation and experimental results come from the simplifications done to the components. The modeling of the PCBs was quite simplified. Many of the components attached to the PCBs have different material properties than the PCB itself, but the model was simplified to be made from a single material. Many components were also removed in the modeling process, such as wires and parts with complex geometries which do not significantly affect the results.

The experimental results were conducted with a large aluminum jig which the machine was attached to. Most of the simulation results did not include the jig. The behavior of introducing the jig was evaluated in the sensitivity analysis where it showed no effect on modal results but seemed to introduce slight damping to the system. As the simulated drive is on the smaller scale of the product families frame sizes, the effect of simulating the jig might become more pronounced.

Many of the connections in the plastic framing are complicated to model accurately. Many snap-on fits are used and some space between the components is present. Modeling each component using accurate contacts would be difficult and resource intensive and could require the use of nonlinear connections. The use of more rigid connections helps with the complexity of the calculations but possibly reduces the accuracy.

The damping coefficient used in the simulation was not based on experimental testing, but rather general estimation based on previously conducted simulations and experiment adjustment according to the sensitivity analysis and comparing to the experimental results.

The machine had connecting wiring in the experimental results, which are not present in the simulation. The stiffness from these cables does affect the results in some ways and is an aspect that was not modelled.

The exact location of the sensor in the experimental testing was not available, which in turn reduces the accuracy of the simulation results. The measurement location can affect the results significantly, as concluded in the sensitivity analysis. Only using this specific testing setup with one measurement location also provides less accuracy and reliability than when using multiple measurement points around the machine.

6 Conclusions

The main goal of the thesis was to find out how vibration simulation correlates with actual measured environmental vibration. Additionally, the sensitivity of such simulation was measured and evaluated through a sensitivity analysis. Lastly the limitations and shortcomings of the methods used were evaluated and discussed.

The results and analysis of the case study concluded that the amplitudes and natural frequencies of the simulation do correlate with the experimental results. The final results showed a clear correlation, especially with the amplitudes of the lowest mode and the natural frequencies in general. The natural frequencies had a maximum absolute error of under 6% and a maximum amplitude absolute error of under 10%. This is not significantly higher than the reported ±5% error in the experimental results.

The results of the sensitivity analysis demonstrated that certain parameters can significantly affect the simulation. Sensitivity analysis was used to expose abnormal behaviors, detecting which would be difficult without the comparison of different parameters.

The findings demonstrate the ability of vibration simulation to predict the behavior of electrical equipment such as the variable frequency drive. Comparing the simulation to the experimental results shows how the validity of the simulation supports actual behavior. Product development stands to benefit from the simulation if good validity models can be achieved in similar products without initial experimental testing. This would allow for cost savings and a more rapid prototyping phase of development.

The research had many assumptions and simplifications that limited the accuracy and reliability of the results. Time constraints made approaching higher levels of detail in the simulation model unattainable. Furthermore, the high sensitivity of the system limits achieving higher levels of accuracy.

Future research on the subject could focus on utilizing the simulation in additional ways than simple harmonic analysis. Research on how a process would work where initial simulation is done to simulate the design phase without experimental results. Based on initial simulation results necessary structural changes or improvements could be made. The changes could be made to change the natural frequencies or amplitudes of the system. This could also be

simulated, multiple versions of improvements could be examined, and the best one could be selected. Such research would be good to validate afterwards in experimental testing.

The effect of more accurate material modeling could further be researched, especially the composite material components. This could provide further accuracy especially since many of the main structural components use composite plastic. Further improvement could come from assigning material level damping as the global damping estimation leaves room for improvement. The magnitude of the more detailed approach could be quantified by the research.

Having standard practices for modeling of the VFD would help in creating multiple simulations across a similar product range. Research on creating a comprehensive reference sensitivity analysis would be beneficial in helping to create a larger number of similar simulations. Additionally, detailed documenting the joint types for individual components, and especially common component pairs would be beneficial for improving the simulation development process. Introduction of the jig was evaluated in the study, but future research on the significance of its effect on the simulation could be researched, especially when simulating heavier VFDs.

Implementation of more complex joint types of especially ones where plastic is used could be investigated. The computational cost of more complex joints and the gained accuracy in comparison to more simplified alternatives could be measured. The use of more localized vibration modeling could be considered. For example, vibration effects on critical individual electric components could be beneficial in the reliability testing of drives.

The results and discussion in the thesis provide an overview of the accuracy and requirements of conducting vibration simulation of environmental vibrations on a variable frequency drive. The benefits and drawbacks are discussed, and areas for future improvement and research are considered.

References

Ansys 2023. Ansys Mechanical User's Guide 2023 R2. [web document]. July 2023 [Referred: 21.5.2024]. 2376 p. + appendixes 103 p.

Ansys 2024a. ANSYS Mechanical. [Ansys webpage]. [Referred: 25.6.2024]. Available at: https://www.ansys.com/products/structures/ansys-mechanical.

Ansys 2024b. What is APDL? [Ansys webpage]. [Referred: 25.6.2024]. Available at: https://www.ansys.com/blog/what-is-apdl.

Ansys 2024c. Ansys SpaceClaim. [Ansys webpage]. [Referred: 25.6.2024]. Available at: https://www.ansys.com/products/3d-design/ansys-spaceclaim.

Ansys 2024d. Ansys Workbench. [Ansys webpage]. [Referred: 25.6.2024]. Available at: https://www.ansys.com/products/ansys-workbench.

Bose, B. K. 1997. Power Electronics and Variable Frequency Drives: Technology and Applications. Piscataway, New Jersey: IEEE Press. 660 p.

Brandt, A. 2010. Noise and Vibration Analysis: Signal Analysis and Experimental Procedures. Newark: Wiley. 464 p.

Bruetsch, A. P., Delima, W. J., Harvie, J. & Harvie, J. 2023. Finite element simulation of electromagnetic shaker for environmental test. Dynamic Environments Testing, Volume 7. Switzerland: Springer. Pp. 87–89.

Cai, L. 2016. Fundamentals of Mechanical Vibrations. Chichester, West Sussex, England: Wiley. 480 p.

Cianetti, F., Morettini, G., Palmieri, M. & Zucca, G. 2019. Virtual qualification of aircraft parts: test simulation or acceptable evidence? Procedia Structural Integrity, 24. Pp. 526-540.

Dong, Y. & Shang, Y. 2019. Virtual simulation test of on-board electronic equipment under mechanical environment. IEEE. Pp. 169-173.

Gorskii, Y. A., Gavrilov, P. A. & Borovkov, A. I. 2020. Virtual proving ground for aircraft structures. IOP Conference Series: Materials Science and Engineering, 986(1), 12020. Pp. 1-12.

Guerrero, J. M., Sasikumar, A., Llobet, J. & Costa, J. 2023. Experimental and virtual testing of a composite-aluminium aircraft wingbox under thermal loading. Aerospace Science and Technology, 138, 108329. Pp. 1-18.

He, J. & Fu, Z. 2001. Modal Analysis. Oxford: Butterworth-Heinemann. 304 p.

IEC 2007. IEC 60068-2-6: Environmental testing – Part 2-6: Tests – Test Fc: Vibration (sinusoidal). Geneva: International Electrotechnical Commission. 82 p.

Kurowski, P. 2016. Finite Element Analysis for Design Engineers, Second Edition. 2nd edition. Warrendale: SAE International. 331 p.

Könözsy, L. 2020. A New Hypothesis on the Anisotropic Reynolds Stress Tensor for Turbulent Flows. Switzerland: Springer International Publishing AG. Pp. 431-432

Lee, Y. C., Wang, B. T., Lai, Y. S., Yeh, C. L., & Chen, R. S. 2008. Finite element model verification for packaged printed circuit board by experimental modal analysis. Microelectronics Reliability 48(11-12). Pp. 1837–1846.

Louback, E., Mistry, J., Azer, P. & Bilgin, B. 2022. Dynamic vibrational analysis of a traction inverter housing. 2022 IEEE Transportation Electrification Conference and Expo, ITEC 2022. P. 7-12.

Martino, J. & Harri, K. 2019. Two-port modeling and simulation of an electrodynamic shaker for virtual shaker testing applications. Journal of Sound and Vibration, 460, 114835. Pp. 1-15.

Palazzolo, A. 2016. Vibration Theory and Applications with Finite Elements. Wiley-Blackwell. 976 p.

Palmieri, M., Cianetti, F., Zucca, G., Morettini, G. & Braccesi, C. 2021. Spectral analysis of sine-sweep vibration: A fatigue damage estimation method. Mechanical Systems and Signal Processing, 157, 107698. Pp. 1-12.

Remedia, M., Aglietti, G., Appolloni, M., Cozzani, A. & Kiley, A. 2017. An enhanced methodology for spacecraft correlation activity using virtual testing tools. Journal of Sound and Vibration, 409. Pp. 180-200.

Remedia, M., Aglietti, G. & Kiley, A. 2015. Vibration testing: post-test correlation approach based on virtual testing. Proceedings of the 29th Aerospace Testing Seminar. October 2015. Los Angeles, California, USA. P. 1-11.

Sahkonumerot 2024. Taajuusmuuttaja General Purpose - ACS580 4kW 400V 9.4A IP55 - ABB Drives. [STK webpage]. [Referred: 23.9.2024]. Available at: https://www.sahkonumerot.fi/3804253/.

Steinberg, D. S. 2000. Vibration Analysis for Electronic Equipment. Wiley Interscience Imprint. 440 p.